Resource

Cell

# Editing DNA Methylation in the Mammalian Genome

## Graphical Abstract

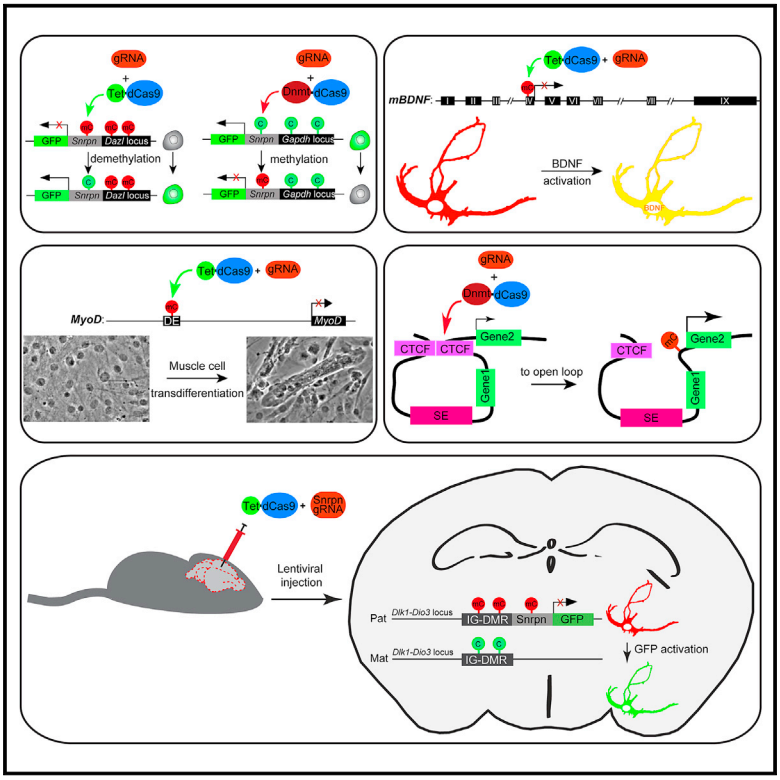


## Authors

X. Shawn Liu, Hao Wu, Xiong Ji, ..., Daniel Dadon, Richard A. Young, Rudolf Jaenisch

## Correspondence

jaenisch@wi.mit.edu

## In Brief

DNA methylation patterns can be specifically altered in mammalian cells using CRISPR/Cas9-based approaches.

## Highlights

- dCas9-Tet1 and -Dnmt3a enable precise editing of CpG methylation in vitro and in vivo
- Targeted demethylation of *BDNF* promoter IV activates BDNF in neurons
- Targeted enhancer demethylation facilitates MyoD-induced muscle cell reprogramming
- Targeted de novo methylation of CTCF motifs alters CTCF-mediated gene loops

Liu et al., 2016, Cell *167*, 233–247
September 22, 2016 
http://dx.doi.org/10.1016/j.cell.2016.08.056

CellPress

Resource

Cell

# Editing DNA Methylation in the Mammalian Genome

X. Shawn Liu,[1,4] Hao Wu,[1,4] Xiong Ji,[1,5] Yonatan Stelzer,[1] Xuebing Wu,[1] Szymon Czauderna,[1,3] Jian Shu,[1] Daniel Dadon,[1,2] Richard A. Young,[1,2] and Rudolf Jaenisch[1,2,6,*]

[1]Whitehead Institute for Biomedical Research, Cambridge, MA 02142, USA

[2]Department of Biology, Massachusetts Institute of Technology, Cambridge, MA 02142, USA

[3]Department of Medical Biotechnology, Faculty of Biochemistry, Biophysics, and Biotechnology, Jagiellonian University, 31-007 Kraków, Poland

[4]Co-first author

[5]Present address: School of Life Sciences, Peking-Tsinghua Center for Life Sciences, Peking University, Beijing 100871, China

[6]Lead Contact

*Correspondence: jaenisch@wi.mit.edu

http://dx.doi.org/10.1016/j.cell.2016.08.056

## SUMMARY

**Mammalian DNA methylation is a critical epigenetic mechanism orchestrating gene expression networks in many biological processes. However, investigation of the functions of specific methylation events remains challenging. Here, we demonstrate that fusion of Tet1 or Dnmt3a with a catalytically inactive Cas9 (dCas9) enables targeted DNA methylation editing. Targeting of the dCas9-Tet1 or -Dnmt3a fusion protein to methylated or unmethylated promoter sequences caused activation or silencing, respectively, of an endogenous reporter. Targeted demethylation of the *BDNF* promoter IV or the *MyoD* distal enhancer by dCas9-Tet1 induced BDNF expression in post-mitotic neurons or activated MyoD facilitating reprogramming of fibroblasts into myoblasts, respectively. Targeted de novo methylation of a CTCF loop anchor site by dCas9-Dnmt3a blocked CTCF binding and interfered with DNA looping, causing altered gene expression in the neighboring loop. Finally, we show that these tools can edit DNA methylation in mice, demonstrating their wide utility for functional studies of epigenetic regulation.**

## INTRODUCTION

Mammalian DNA methylation at 5-cytosine plays critical roles in many biological processes, including genomic imprinting, cell-fate determination, chromatin architecture organization, and regulation of gene expression (Bird, 2002; Jaenisch and Bird, 2003; Smith and Meissner, 2013). Genetic studies have revealed that DNA methylation is essential for mammalian development and adaptation to environmental signals (Jaenisch and Bird, 2003). Abnormal DNA methylation has been observed in cancer and neurological disorders (Robertson, 2005). Owing to the advancement in sequencing technologies, single-nucleotide resolution methylation maps for many types of human and mouse cells and tissues have been depicted (Lister et al., 2009, 2013). Importantly, these maps have allowed for the identification of differentially methylated regions (DMRs) at base pair resolution during different stages of normal development as well as disease (De Jager et al., 2014; Landau et al., 2014). However, investigation of the functional significance of these DMRs remains a challenge due to lack of appropriate molecular tools that enable efficient editing of DNA methylation in a targeted manner.

We set out to establish such a toolbox by hybridization of the key enzymes in the DNA methylation pathway with reprogrammable sequence-specific DNA-targeting molecular machinery. DNA methylation is established by two de novo DNA methyltransferases (Dnmt3a/b) and is maintained by Dnmt1 (Smith and Meissner, 2013). Gene activation during development is associated with demethylation of promoter and enhancer sequences with the best-understood mechanism being passive demethylation by inhibition of Dnmt1. In addition, demethylation can be achieved through oxidation of the methyl group by TET (ten-eleven translocation) dioxygenases to form 5-hydroxymethylcytosine (5-hmC), and then restoration into unmodified cytosines by either DNA replication-dependent dilution or DNA glycosylase-initiated base excision repair (BER), a process termed as active demethylation and proposed to operate during specific developmental stages such as preimplantation embryos or in post-mitotic neurons (Wu and Zhang, 2014).

Clustered regularly interspaced palindromic repeats (CRISPR), a type II bacterial adaptive immune system, has been modified to target the Cas9 nuclease to the desired genomic loci with sequence-specific guide RNAs for genome editing (Cong et al., 2013; Jinek et al., 2012; Mali et al., 2013). Importantly, a catalytically inactive Cas9 (dCas9) was generated and engineered in several systems as a DNA targeting module to bring effector proteins such as transcriptional activator/suppressor, chromatin modifier, and green fluorescence protein to regulate gene expression, to modify chromatin, and to image genomic loci respectively (Chen et al., 2013; Gilbert et al., 2013; Hilton et al., 2015; Jinek et al., 2012; Konermann et al., 2015; Qi et al., 2013).

In this study, we demonstrate that fusion of dCas9 with the Tet1 enzymatic domain or Dnmt3a allows for targeted erasure or establishment of DNA methylation, respectively. As a proof of principle, we first induced alterations to DNA methylation in two synthetic methylation reporters integrated in mouse embryonic stem cells (mESCs). We further show that targeted demethylation of *BDNF* promoter IV is sufficient to activate its expression in mouse cortical neurons, and that targeted

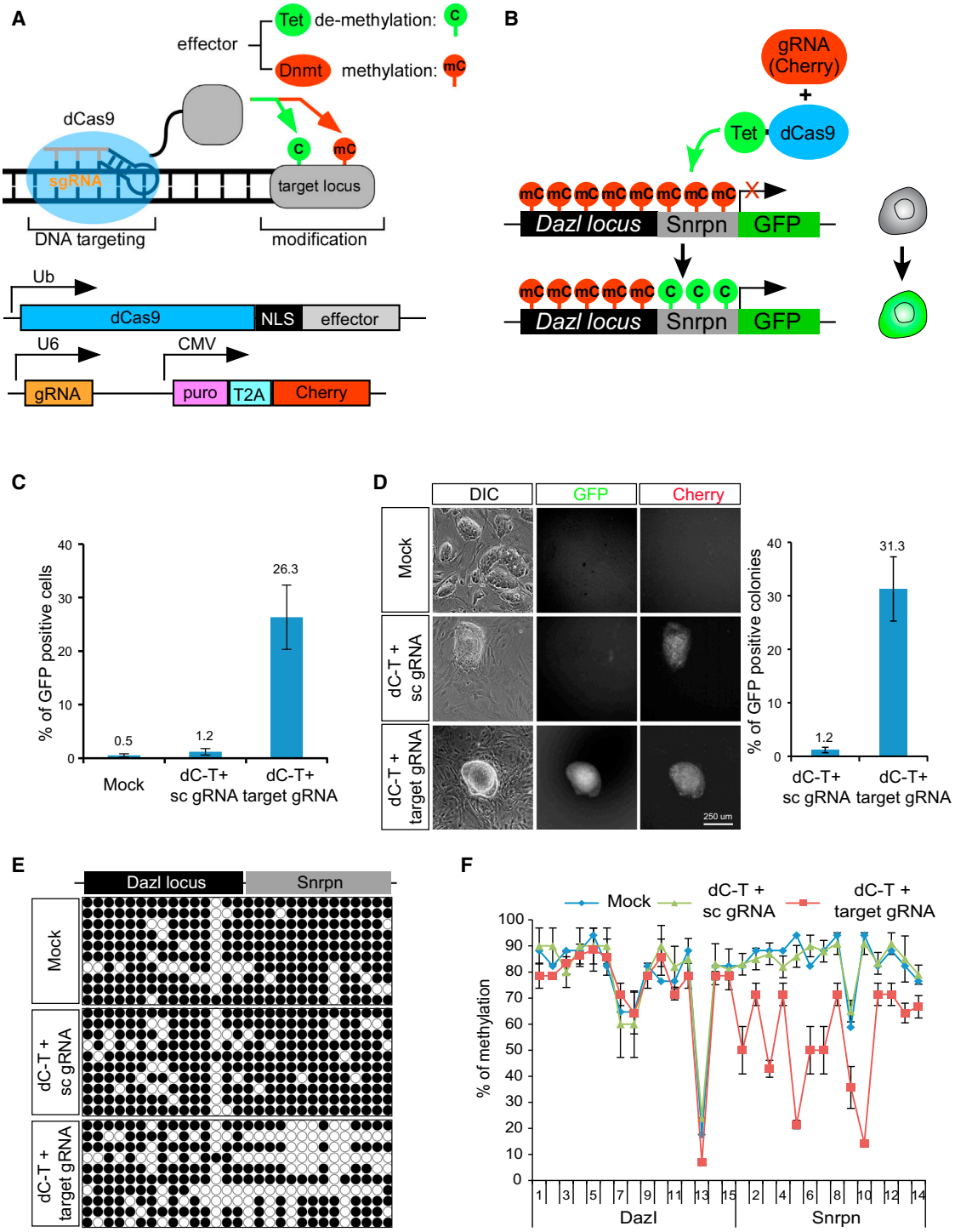


**Figure 1. Activation of the Dazl-Snrpn-GFP Reporter by dCas9-Tet1**

(A) Upper panel: schematic representation of a catalytically inactive mutant Cas9 (dCas9) fused with Tet1 for erasing DNA methylation, and with Dnmt3a for de novo methylation of specific sequences. Lower panel: an optimized dCas9-effector construct and a guide RNA (gRNA) construct with *puro* and *Cherry* cassettes.

(B) Schematic representation of targeting the *Snrpn* promoter region by dCas9-Tet1 with specific gRNAs to erase methylation and activate GFP expression.

(C) Dazl-Snrpn-GFP mESCs were infected with lentiviruses expressing dCas9-Tet1 (dC-T) with a scrambled gRNA (sc gRNA) or four gRNAs targeting the *Snrpn* promoter region (target gRNA). Percentages of GFP positive cells were calculated by flow cytometric analysis of these cells 3 days post-infection and shown as the mean percentages of GFP positive cells ±SD of two biological replicates. Note that the percentages of GFP-positive cells are expressed as the fraction of infected Cherry-positive cells.

*(legend continued on next page)*

demethylation of a *MyoD* distal enhancer promotes reprogramming of fibroblasts into myoblasts and facilitates myotube formation. With dCas9-Dnmt3a, we demonstrate that targeted methylation at CTCF binding sites is able to block CTCF recruitment and to alter the expression of genes in the neighborhood loop by increasing their interaction frequencies with the super-enhancers insulated in the targeted loops. Furthermore, lentiviral delivery of dCas9-Tet1 with target gRNAs into mice enabled in vivo activation of a methylation reporter by demethylation of its promoter. Thus, dCas9-Tet1 and dCas9-Dnmt3a provide powerful tools to investigate the functional significance of DNA methylation in a locus-specific manner.

## RESULTS

### A Modified CRISPR System to Edit DNA Methylation

To achieve targeted editing of DNA methylation, we fused dCas9 with enzymes in the methylation/demethylation pathway (Figure 1A). Based on previous studies using the TALE system to target specific CpGs (Bernstein et al., 2015; Maeder et al., 2013), Tet1 and Dnmt3a were chosen as the effectors in our system. Co-expression of sequence-specific guide RNA (gRNA) would be expected to target dCas9-Tet1 or dCas9-Dnmt3a to the specific locus and mediate modification of DNA methylation status without altering the DNA sequence. To optimize this chimeric CRISPR/dCas9-effector system, we tested two types of dCas9-Tet1 lentiviral constructs with nuclear localization signal (NLS) at different positions: dCas9-NLS-Tet1 and NLS-dCas9-NLS-Tet1 (Figures S1A and S1B). We also tested two types of gRNA lentiviral constructs, a widely used chimeric single-guide RNA referred to as gRNA (Jinek et al., 2012) and a modified guide RNA with enhanced capacity to guide Cas9 to the designed genomic locus referred to as E-gRNA (Chen et al., 2013). Both gRNA constructs contain a *puro* selection cassette and a Cherry fluorescence protein cassette driven by an independent CMV promoter that allows for fluorescence activated cell sorting (FACS) of gRNA-expressing cells after lentiviral transduction (Figure S1A). Characterization of these constructs showed a robust gRNA-induced nuclear translocation for the dCas9-NLS-Tet1 construct (Figures S1C–S1E), and thus this construct was chosen for all experiments in order to minimize non-specific modifications of DNA. Two types of gRNA behaved similarly (Figures S1C–S1E) and thus were used interchangeably.

### dCas9-Tet1 and dCas9-Dnmt3a Enable Targeted Alterations of CpG Methylation State

To assess whether the dCas9-Tet1 and -Dnmt3a fusion constructs would induce demethylation or de novo methylation, respectively, of specific sequences, we utilized a methylation reporter system previously developed in our laboratory (Stelzer et al., 2015). This reporter system consists of a synthetic methylation-sensing promoter (conserved sequence elements from the promoter of an imprinted gene, *Snrpn*) that controls the expression of a GFP. Insertion of this reporter construct into a genomic locus was shown to faithfully report on the methylation state of the adjacent sequences (Stelzer et al., 2015).

#### *Demethylation of Specific CpGs*

To test whether defined sequences could be demethylated, we introduced the dCas9-Tet1 construct in combination with gRNAs to target the Snrpn-GFP reporter inserted into the *Dazl* promoter (Figure 1B). *Dazl* is a germ cell specific gene, which is hypermethylated and not active in ES cells, and thus the GFP reporter is not expressed. To activate GFP expression by dCas9-Tet1, we designed four gRNAs targeting all 14 CpGs in the *Snrpn* promoter region (Figure S2A). After infection with lentiviral vectors co-expressing dCas9-Tet1 and the four gRNAs for 3 days, some infection-positive cells as labeled by Cherry positive signal expressed from gRNA construct began to turn on GFP (Figure S2B). To assess the activation efficiency by dCas9-Tet1 with target gRNAs, we analyzed the cells infected by both viruses using FACS. Among the Cherry positive population, about 26% of cells with target gRNAs activated GFP, whereas only 1% of cells with a scrambled gRNA were GFP positive (Figures 1C and S2C). These Cherry positive single cells were further cultured to allow for formation of ES cell colonies. Cells with target gRNAs, but not the scrambled gRNA, expressed GFP (Figure 1D). To confirm that the activation of GFP in these cells is caused by demethylation of the *Snrpn* promoter, we performed bisulfite sequencing of genomic DNA from these samples. As illustrated in Figures 1E and 1F, samples from cells with target gRNAs showed robust demethylation only in the *Snrpn* promoter region but not the adjacent *Dazl* locus, and samples from the cells with the scrambled gRNA showed a similar methylation status to the uninfected (mock) control. We further analyzed the GFP-positive and -negative populations within infected Cherry-positive cells. As shown in Figure S2D, a more robust demethylation of the *Snrpn* promoter region was observed in double-positive cells ($Cherry^+$;$GFP^+$). These results confirm the targeted erasure of DNA methylation by dCas9-Tet1 with gRNAs in proliferative cells.

#### *De Novo Methylation of Specific CpGs*

To assess whether a dCas9-Dnmt3a fusion protein could de novo methylate promoter sequences and silence gene expression, we used cells carrying the Snrpn-GFP reporter in the *Gapdh* promoter. These cells are GFP positive because *Gapdh* is unmethylated and expressed in ES cells (Stelzer et al., 2015). We infected the Gapdh-Snrpn-GFP ESCs with lentiviruses expressing dCas9-Dnmt3a and gRNAs targeting the *Snrpn* promoter or a scrambled gRNA (Figures 2A and S2E), followed by FACS analysis. Among infection-positive (Cherry-positive) population, about 12% of cells with target gRNAs inactivated GFP, whereas only 2% of cells with the scrambled gRNA were GFP negative (Figures 2B and S2F). When the Cherry positive cells were grown in culture,

(D) Left, representative fluorescence images of the sorted Cherry positive cells in (C) after culturing for 1 week. Scale bar, 250 μm. Right, percentages of GFP positive colonies were quantified and shown as the mean percentages of GFP positive colonies ±SD of two biological replicates.

(E) Bisulfite sequencing of cells described in (C).

(F) Methylation levels of individual CpGs in the *Snrpn* promoter region and the adjacent *Dazl* locus. Shown is the mean percentage ±SD of two biological replicates.

See also Figures S1 and S2.

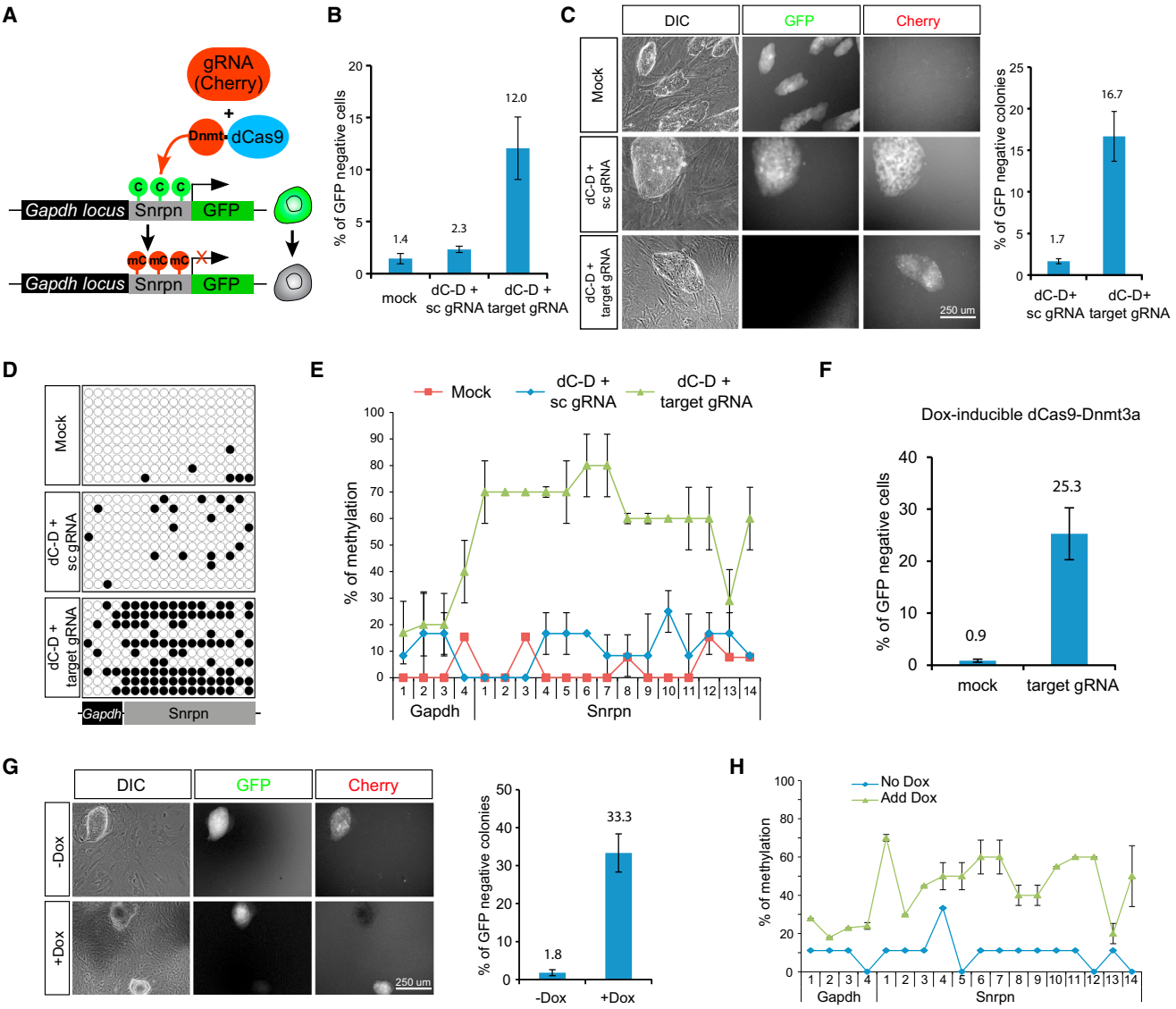


**Figure 2. Silencing of the Gapdh-Snrpn-GFP Reporter by dCas9-Dnmt3a**

(A) Schematic representation of targeting the *Snrpn* promoter region by dCas9-Dnmt3a with specific gRNAs to methylate the promoter and silence GFP expression.

(B) Gapdh-Snrpn-GFP mESCs were infected with lentiviruses expressing dCas9-Dnmt3a (dC-D) with a scrambled gRNA (sc gRNA) or gRNAs targeting the *Snrpn* promoter region (target gRNA). Percentage of GFP negative cells was calculated by flow cytometric analysis 3 days after infection and is shown as the mean percentages of GFP negative cells ±SD of two biological replicates. Note that the percentages of GFP-positive cells are expressed as the fraction of infected Cherry-positive cells.

(C) Left, representative fluorescence images of the sorted Cherry-positive cells in (B) after culturing for 1 week. Scale bar, 250 μm. Right, percentages of GFP negative colonies were quantified and are shown as the mean percentages of GFP negative colonies ±SD of two biological replicates.

(D) Bisulfite sequencing of cells described in (B).

(E) Methylation levels of individual CpGs in the *Snrpn* promoter region and the adjacent *Gapdh* locus. Shown is the mean percentage ±SD of two biological replicates.

(F) Gapdh-Snrpn-GFP mESCs with Doxycycline-inducible dCas9-Dnmt3a were infected with lentiviruses expressing gRNAs targeting the *Snrpn* promoter region in the presence of Doxycycline (2 μg/ml). Percentages of GFP negative cells were calculated by flow cytometric analysis 3 days after infection and are shown as the mean percentages of GFP negative cells ±SD of two biological replicates. Note that the percentages of GFP-negative cells are expressed as the fraction of infected Cherry-positive cells.

(G) Left, representative fluorescence images of the sorted Cherry-positive population in (F) after culturing for 1 week with or without Doxycycline. Scale bar, 250 μm. Right, percentages of GFP negative colonies were quantified and are shown as the mean percentages of GFP negative colonies ±SD of two biological replicates.

(H) Methylation level of each individual CpGs in the *Snrpn* promoter region and the adjacent *Gapdh* locus from cells in (G). Shown is the mean percentage ±SD of two biological replicates.

See also Figure S2.

GFP expression of cells with target gRNAs remained off whereas cells with the scrambled gRNA and mock controls remained GFP positive (Figure 2C). Furthermore, bisulfite sequencing showed that transduction of dCas9-Dnmt3a/gRNAs resulted in a significant increase of DNA methylation in the *Snrpn* promoter region but not in the adjacent *Gapdh* region (Figures 2D and 2E). Further analysis of the GFP-positive and -negative populations within infected Cherry-positive cells showed a more robust methylation of the *Snrpn* promoter region in Cherry$^+$;GFP$^-$ cells (Figure S2G). To overcome the possible limitation caused by low co-transduction efficiency of both dCas9-Dnmt3a and gRNA lentiviruses, a Doxycycline-inducible dCas9-Dnmt3a expression cassette was integrated into the Gapdh-Snrpn-GFP mES cell line by using a PiggyBac transposon system (Figure S2H). After delivery of the same group of target gRNAs, FACS analysis showed that GFP inactivation efficiency was increased to 25% (Figures 2F and S2I). Sorted Cherry-positive cells showed loss of GFP expression upon Doxycycline treatment (Figure 2G) and were robustly methylated in the *Snrpn* promoter region (Figure 2H). We also generated a new construct of dCas9-Dnmt3a-P2A-BFP, which enables isolation of dCas9-Dnmt3a-expressing cells by FACS. ~70% of GFP inactivation efficiency was achieved in FACS sorted double-positive cells (BFP$^+$;Cherry$^+$) after lentiviral delivery of this construct together with gRNAs (Figure S2J).

In summary, our results indicate that the dCas9 fusion constructs described above either efficiently demethylate methylated sequences (dCas9-Tet1) or de novo methylate unmethylated sequences (dCas9-Dnmt3a) in dividing cells when targeted by specific guide RNAs.

## Comparison of dCas9- and TALE-Based Methylation Editing

To compare the methylation editing efficacy and effective range by dCas9-Tet1/Dnmt3a with TALE-based methods, we chose two previously reported loci edited by TALE-based method (Bernstein et al., 2015; Maeder et al., 2013) and designed a single gRNA targeting dCas9-Tet1/Dnmt3a to the same site bound by the TALE-Tet1/Dnmt3a. As shown in Figures S3A and S3C, dCas9-Dnmt3a with one single gRNA targeting the *p16* locus induced an average of a 25% increase of methylation within a 320-bp region of the *p16* promoter, whereas TALE-Dnmt3a only induced a 13% increase within a 650-bp region. Similarly, dCas9-Tet1 with one single gRNA targeting the *RHOXF2* locus induced an average of a 28% decrease of methylation within a 150-bp region of the *RHOXF2* promoter, whereas TALE-Tet1 only induced a 14% decrease within a 200-bp region (Figures S3B and S3C). These results suggest that the dCas9-Tet1/Dnmt3a system has higher efficacy and resolution for methylation editing than the TALE-based method.

To evaluate the specificity of dCas9-Tet1/Dnmt3a-mediated methylation editing, we performed a dCas9 chromatin immunoprecipitation sequencing (ChIP-seq) assay and identified nine binding sites in the presence of gRNAs targeting the *Dazl-Snrpn* region described in Figure S2A and 18 binding sites in the presence of gRNAs targeting CTCF binding sites adjacent to the *miR290* locus (see below Figure S6A). Figure S3D shows that among the identified binding sites for each group of gRNAs, the targeted locus (*Dazl-Snrpn* or *miR290*) showed the highest level of binding for dCas9-Tet1/Dnmt3a (Table S1). The second and third strongest binding sites for each targeted locus were illustrated in Figure S3E, and bisulfite sequencing analysis of these loci showed only marginal change in methylation level (Figures S3F and S3G), likely due to the significantly lower binding affinity of dCas9-Dnmt3a/Tet1 at these off-target loci compared to the targeted loci. These results indicate that dCas9-based epigenetic editing can be highly specific.

## Targeted Demethylation of *BDNF* Promoter IV Activates BDNF in Neurons

DNA replication-independent active demethylation has been proposed to operate in post-mitotic neurons (Guo et al., 2011; Martinowich et al., 2003). To test whether active demethylation can be induced in post-mitotic neurons, we applied the dCas9-Tet1 system to study the regulation of the *BDNF* gene. BDNF expression can be induced by neuronal activity accompanied by demethylation of its promoter IV (Chen et al., 2003; Martinowich et al., 2003). We designed four gRNAs targeting 11 CpGs in the *BDNF* promoter IV (Figure S4A) to determine whether dCas9-Tet1 can activate BDNF by inducing demethylation of this promoter (Figure 3A). Mouse cortical neurons were isolated from E17.5 embryos and cultured for 2 days in vitro (DIV2) following a well-established experimental procedure for producing primary neuronal culture (Ebert et al., 2013). As shown in Figures S4B–S4D, KCl treatment induced BDNF expression in these neurons with no detectable cell proliferation. Neurons at day 3 in culture (DIV3) were infected with lentiviral vectors expressing dCas9-Tet1 with or without the four gRNAs at almost 100% transduction efficiency (Figure S4E). At 48 hr post-infection some of the cultures were treated with KCl to induce neuronal activity. As shown in Figures 3B and 3C, dCas9-Tet1/gRNAs induced BDNF expression by about 6-fold, whereas dCas9-Tet1 in the absence of gRNAs showed only a slight induction (less than 2-fold) and a catalytically dead form of Tet1 (dC-dT) showed no induction. Importantly, the same group of dCas9-Tet1/gRNAs did not induce *Npas4* expression (Figure S4F), another neuronal activity-inducible gene (Lin et al., 2008). Co-transduction of dCas9-Tet1 with each individual gRNA targeting the *BDNF* promoter IV showed a 2- to 3-fold induction of BDNF (Figure S4G). We performed bisulfite sequencing to examine the methylation state of *BDNF* promoter IV. As shown in Figures 3D and 3E, dCas9-Tet1/gRNAs significantly reduced methylation in this region in contrast to gRNA negative controls while KCl treatment also induced demethylation of CpGs at positions of −148, −66 and, −19 (relative to transcription start site).

Our results demonstrate that demethylation of the *BDNF* promoter IV can be induced by dCas9-Tet1/gRNAs and is sufficient to activate BDNF expression. Because post-mitotic neurons were used for these experiments, loss of methylation was likely due to active demethylation. To further support this conclusion, we examined 5-hmC levels in the *BDNF* promoter IV during the time course of dCas9-Tet1 induced demethylation by Tet-assisted Bisulfite sequencing (TAB-seq) analysis. As shown in Figure S4H, 5-hmC was detected 40 hr post-infection with dCas9-Tet1 and gRNA lentiviruses and diminished after 60 hr. Similarly, 5-hmC was also detected after KCl treatment (Figure S4I). As the bisulfite sequencing method does not distinguish

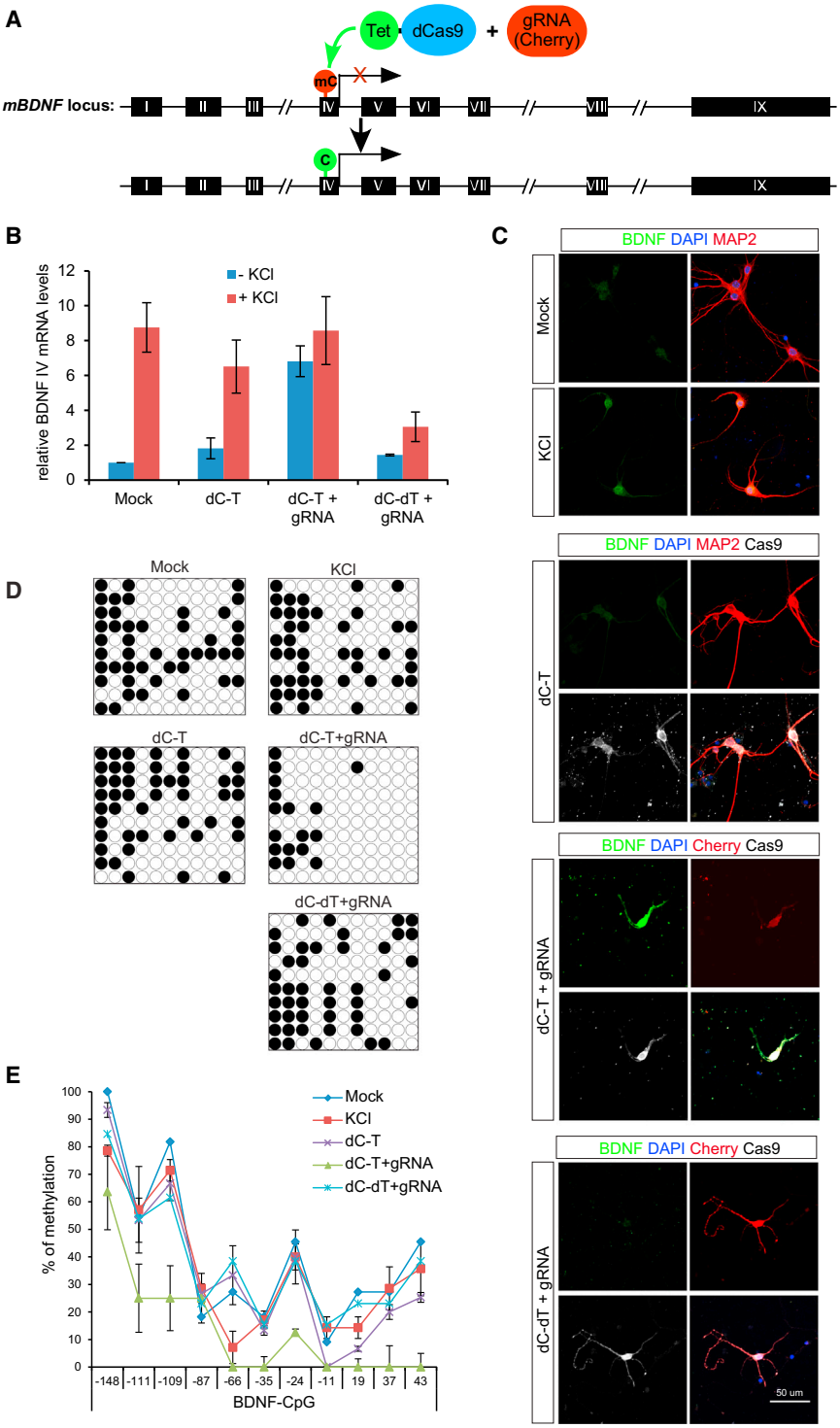


**Figure 3. Targeted Demethylation of *BDNF* Promoter IV by dCas9-Tet1 to Activate BDNF in Neurons**

(A) Schematic representation of targeting *BDNF* promoter IV by dCas9-Tet1 (dC-T) with specific gRNAs to erase methylation and activate BDNF expression.

(B) Mouse cortical neurons cultured in vitro for 3 days (DIV3) were infected with lentiviruses expressing dC-T with or without gRNAs targeting the *BDNF* promoter IV or a catalytically dead form of Tet1 (dC-dT) with *BDNF* gRNAs for 2 days, and then treated with or without KCl (50 mM) for 6 hr before harvesting for RT-qPCR analysis. Bars are mean ±SD of three biological replicates.

(C) Representative confocal images for BDNF induction in (B). Stained in red for MAP2 (top two panels) or Cherry (bottom two panels), green for BDNF, blue for DAPI and gray for dCas9. Scale bar, 50 μm.

(D) Bisulfite sequencing of neurons in (C).

(E) Methylation levels of each individual CpGs in the *BDNF* promoter IV region. Shown is the mean percentage ±SD of two biological replicates.

See also Figure S4.

unmethylated 5-cytosine (5-C) and 5-formlycytosine/5-carboxylcytosin (5-fC/5-caC) generated from 5-hmC, it is possible that some CpGs were 5-fC/5-caC modified after targeting with dCas9-Tet1/gRNA. Nevertheless, inhibition of the base excision repair pathway by treatment with ABT-888 (an inhibitor of PARP) reduced the activation of BDNF by KCl treatment (Figure S4J), suggesting that demethylation of *BDNF* promoter IV contributes to BDNF activation.

To test whether endogenous Tet activity was required to regulate BDNF expression upon neuronal activity stimulation, we treated DIV3 neurons with 2-hydroxygluterate, a competitive inhibitor for α-ketoglutarate-dependent dioxygenases including Tet enzymes (Xu et al., 2011). As shown in Figure S4K, pharmacological inhibition of Tet enzymatic activity completely abolished the induction of BDNF expression by KCl treatment. Furthermore, mouse primary cortical neurons carrying a Tet1-null mutant showed significantly attenuated activation kinetics of BDNF (Figure S4L), supporting a role of endogenous Tet for induction of neuronal activity.

## Targeted Demethylation of the *MyoD* Distal Enhancer Facilitates Myogenic Reprogramming of Fibroblasts

The role of MyoD as a master regulator for muscle development was initially defined by the observations that demethylation of DNA in fibroblasts by 5-Aza (5-Aza-2′-deoxycytidine) treatment resulted in activation of MyoD and subsequent myoblast conversion and myotube formation (Constantinides et al., 1977; Davis et al., 1987; Lassar et al., 1986). Six muscle-specific DMRs have been described within the 50-kb upstream region of *MyoD* gene (Schultz et al.,

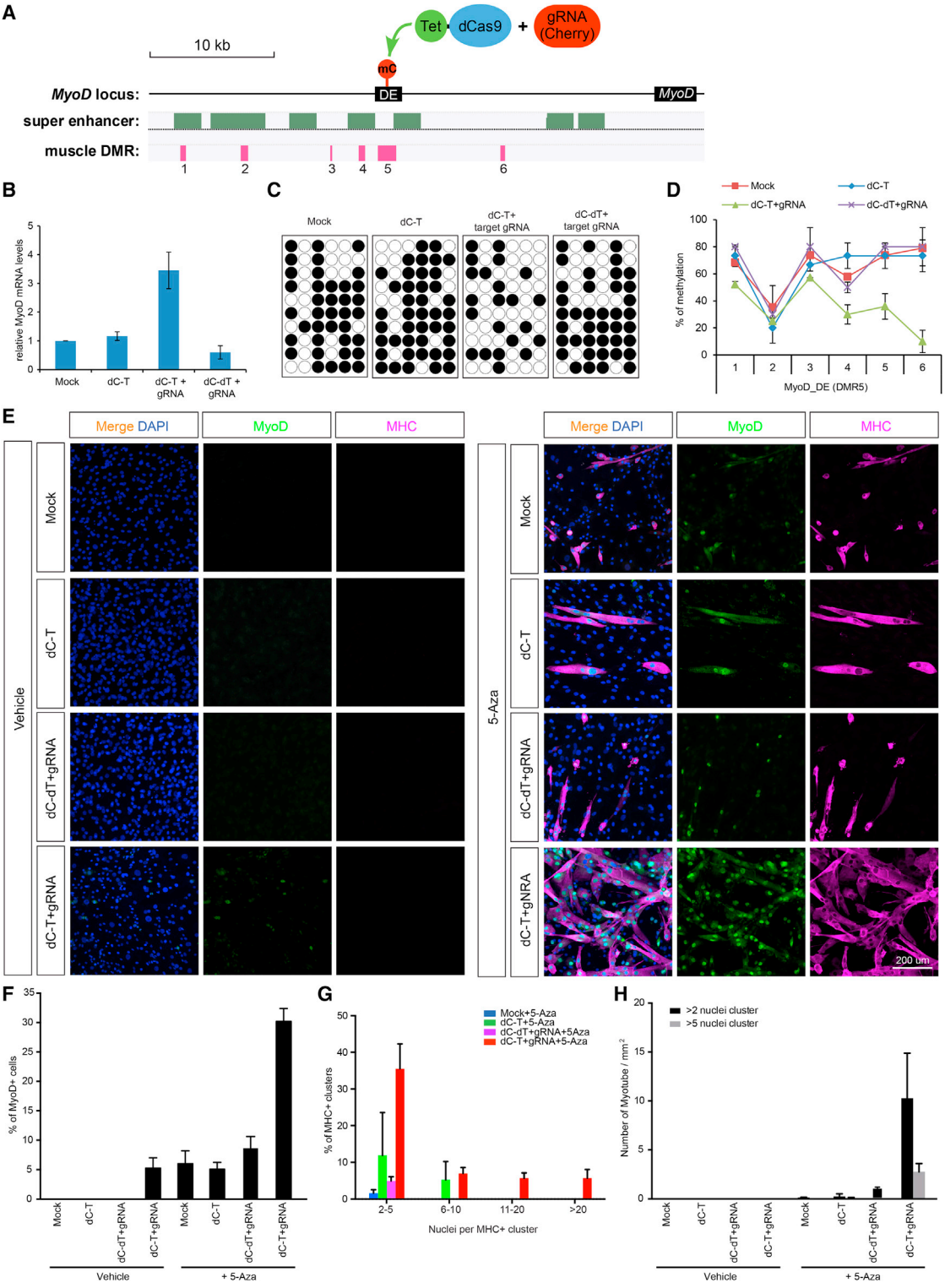


**Figure 4. Targeted Demethylation of the *MyoD* Distal Enhancer by dCas9-Tet1 to Facilitate Conversion of Fibroblasts to Myoblasts**

(A) Schematic representation of targeting the *MyoD* distal enhancer (DE) region in DMR-5 by dCas9-Tet1 (dC-T) with specific gRNAs.

(B) C3H10T1/2 cells were infected with lentiviruses expressing dC-T with target gRNAs, or a catalytically dead form of Tet1 (dC-dT) with target gRNAs for 2 days. Cherry positive cells were FACS sorted for RT-qPCR analysis. Bars represent mean ± SD of three experimental replicates.

(C) Bisulfite sequencing of cells in (B).

*(legend continued on next page)*

2015), and DMR-5 overlaps with a known distal enhancer of *MyoD* (Brunk et al., 1996) as shown in Figure 4A. To test whether demethylation of DMR-5 would activate MyoD in fibroblasts, we designed four gRNAs targeting this DMR (Figure S5A). Co-expression of dCas9-Tet1 with these gRNAs in C3H10T1/2 cells, a sub-clone from mouse embryonic fibroblasts previously used for 5-Aza mediated MyoD activation (Constantinides et al., 1977), resulted in a moderate induction of MyoD expression (3-fold) as shown in Figure 4B. Combination of dCas9-Tet1/*MyoD* DMR-5 gRNAs with 5-Aza treatment resulted in a higher induction of MyoD as shown in Figure S5F. Bisulfite sequencing showed a substantial reduction of methylation in the DMR-5 region of sorted infection-positive cells transduced with dCas9-Tet1 and target gRNAs lentiviruses, but not with a catalytically dead Tet1 (dC-dT) or a scrambled gRNA (Figures 4C and 4D). To investigate whether demethylation of the *MyoD* distal enhancer region could reprogram fibroblasts into muscle cells, we infected C3H10T1/2 cells with lentiviruses expressing dCas9-Tet1 and gRNAs. The cells were cultured for 14 days and analyzed for MyoD and MHC (Myosin Heavy chain, a myotube specific marker) expression. As shown in Figures 4E and 4F, co-expression of dCas9-Tet1 with gRNAs targeting DMR-5 induced a moderate expression level of MyoD but was not sufficient to induce myotube formation in the absence of 5-Aza treatment.

We then investigated whether targeted demethylation of DMR-5 would synergize with 5-Aza treatment to induce myotube formation (Figure S5B). To follow the process of myotube formation after 5-Aza treatment, a time-course experiment was performed. Multi-nucleated myotubes (MHC-positive) with heterogeneous sizes began to form 14 days post-treatment, and both MyoD-positive cell ratio and myotube density and size then increased up to day 25 (Figures S5C–S5E). Co-expression of dCas9-Tet1 with gRNAs targeting *MyoD* DMR-5 facilitated the myotube formation 14 days post-treatment as evidenced by significantly more mature, multi-nucleated $MHC^+$ clusters (>2 nuclei per $MHC^+$ cluster) compared to cells expressing only dCas9-Tet1 or dC-dT with *MyoD* DMR-5 gRNAs (Figures 4E, 4G, and 4H). A similar observation was made when the cells were analyzed at a later time point (16 days) post-treatment (Figures S5G–S5J). Our results suggest that demethylation of the *MyoD* distal enhancer by dCas9-Tet1/gRNA synergizes with 5-Aza in C3H10T1/2 cells to substantially facilitate myoblast conversion and myotube formation.

## Targeted De Novo Methylation of CTCF Binding Sites Alters CTCF-Mediated Gene Loops

CTCF is a highly conserved zinc finger protein that plays a primary role in the global organization of chromatin architecture (Phillips and Corces, 2009). Transcriptional enhancers normally interact with their target genes through the formation of DNA loops (Gibcus and Dekker, 2013; Gorkin et al., 2014; Kagey et al., 2010), which typically are constrained within larger CTCF-mediated loops called insulated neighborhoods (Dowen et al., 2014; Ji et al., 2016; Phillips-Cremins et al., 2013), which, in turn, can form clusters of loops that contribute to topologically associating domains (TADs) (Dixon et al., 2012; Nora et al., 2012). Deletion of the CTCF loop anchor sites of insulated neighborhoods can cause enhancers to interact inappropriately with genes located outside the loop and thus increase their expression (Dowen et al., 2014). Interestingly, methylation of the DNA recognition site of CTCF has been reported to block CTCF binding (Bell and Felsenfeld, 2000; Wang et al., 2012). To study whether methylation of specific CTCF sites could alter CTCF-mediated gene loops, we applied the dCas9-Dnmt3a system to target CTCF anchor sites (Figure 5A). We designed specific gRNAs (Figure S6) targeting dCas9-Dnmt3a to two CTCF sites to investigate whether de novo methylation would interfere with the looping function of CTCF (Figures 5B and 5F). Doxycycline-inducible dCas9-Dnmt3a mES cells (Figure S2H) were infected with lentiviruses expressing the gRNAs and transduced cells were FACS sorted for subsequent analysis.

Targeting of dCas9-Dnmt3a to the CTCF binding site bordering the *miR290* loop that harbors a super-enhancer (Figure 5B) induced de novo methylation of CpGs at this site (Figures 5D and 5E). Gene expression analysis of transduced cells showed a significant elevation of *Nlrp12* gene, which is outside of this super-enhancer-containing insulated neighborhood and next to the targeted CTCF site, but did not affect the expression of genes that are located inside the *miR290* loop or of genes in other neighboring loops including *AU018091* and *Myadm* (Figure 5C). Similarly, targeting of dCas9-Dnmt3a to the CTCF binding site bordering the *Pou5f1* gene loop that harbors another super-enhancer (Figure 5F) induced methylation of CpGs in the CTCF binding sequence (Figures 5H and 5I) and increased the expression of H2Q10, which is located in a neighboring loop and next to the targeted CTCF site but did not affect the expression of the *Pou5f1* gene itself or the *Tcf19* gene in the other neighboring loop (Figure 5G). For either targeted CTCF sites, a catalytically inactive Dnmt3a form (dC-dD) did not induce changes in methylation level or gene expression as did by dC-D (Figures 5C–5E and 5G–5I). These observations are consistent with the results obtained when these CTCF sites were deleted (Dowen et al., 2014) and support the notion that methylation of the CTCF binding site interferes with its insulator function.

To test whether targeted methylations of CTCF binding sites would result in increased interaction frequencies between

(D) Methylation level of individual CpGs in the *MyoD* DE region. Shown is the mean percentage ±SD of two biological replicates.
(E) Representative confocal images for C3H10T1/2 cells on day 14 in the fibroblast-to-myoblast conversion assay. Stained in green for MyoD, magenta for MHC and blue for DAPI. Scale bar, 200 μm.
(F) Quantification of MyoD positive cell ratio 14-day post-infection with lentiviruses expressing dC-T alone, dC-T or dC-dT with gRNAs targeting DMR-5.
(G) Distribution profile of MHC positive cell clusters based on nuclei number per $MHC^+$ cluster (grouped as 2–5, 6–10, 11–20, and >20 nuclei per $MHC^+$ cluster) 14 days post-infection.
(H) Quantification of myotube density in MHC positive clusters with more than two or five nuclei at 14 days after infection. Data are quantified from three to five representative images for (F)–(H). Bars represent mean ± SD.
See also Figure S5.

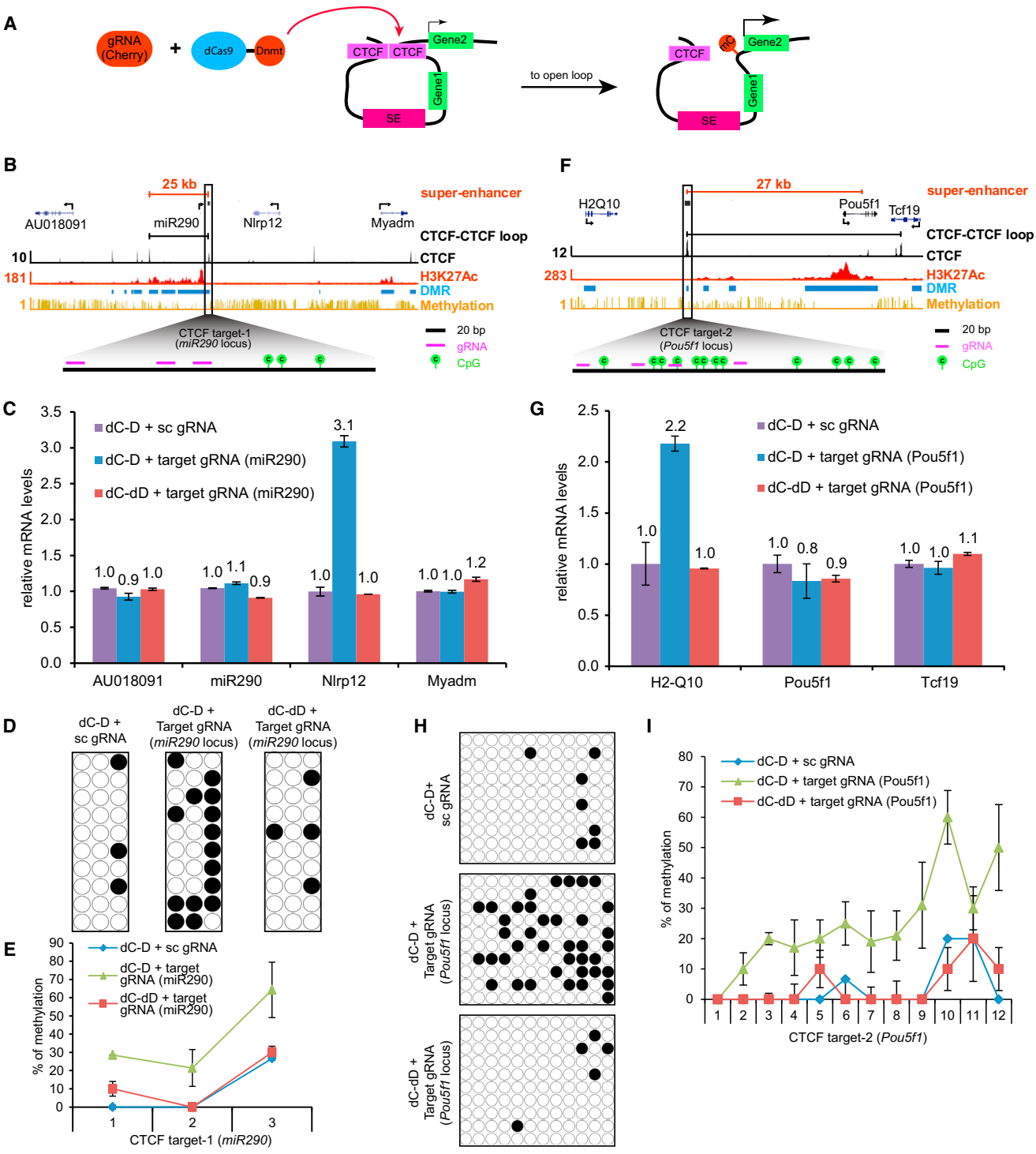


**Figure 5. Targeted Methylation of CTCF Binding Sites**

(A) Schematic representation of targeting the CTCF binding site by dCas9-Dnmt3a with specific gRNAs to induce de novo methylation, block CTCF recruitment, and open CTCF loops, which alters gene expression in the adjacent loop.

(B) Schematic representation of CTCF target-1 (*miR290* locus) with super-enhancer and *miR290* in the loop, *AU018091* gene in the left neighboring loop, and *Nlrp12* gene in the right neighboring loop (close to the targeted CTCF binding site). The *Myadm* gene is in the adjacent loop right to the loop containing *Nlrp12*. The super-enhancer domain is indicated as a red bar. The targeted CTCF site is highlighted with a box. ChIP-seq binding profiles (reads per million per base pair) for CTCF in black and H3K27Ac (super-enhancer) in red, and methylation track in yellow with DMR in blue are also shown.

*(legend continued on next page)*

insulated super-enhancers and activated genes, Chromosome Conformation Capture (3C) assay was performed at these loci. As shown in Figure 6A, the interaction frequency between super-enhancers in the *miR290* loop and the newly activated gene (*Nlrp12*) in the neighboring loop was significantly increased but the interaction between *Nlrp12* and *Myadm* genes remained the same, indicating an open conformation for this targeted CTCF loop. To confirm that the increased interaction frequency was due to blocking CTCF anchoring, we performed a CTCF ChIP assay. Binding of CTCF to the targeted genomic site was significantly reduced in the sample with *miR290* target gRNAs as compared to the sample with a scrambled gRNA, gRNAs targeting other CTCF binding sites, or a catalytically inactive dC-dD with *miR290* target gRNAs (Figure 6B), supporting the notion that DNA methylation blocks CTCF anchoring and thus alters the CTCF loop conformation. A similar set of experiments was performed for the second CTCF loop (*Pou5f1* loop) demonstrating increased interaction frequency between the insulated super-enhancers and the newly activated gene (*H2Q10*) and decreased binding of CTCF after targeted methylation of its binding site (Figures 6C and 6D).

In summary, our results demonstrate that the dCas9-Dnmt3a system can be used to change the methylation state of specific CTCF anchor sites and thus to interfere with the CTCF looping function.

### In Vivo Demethylation of an Endogenous Locus for Gene Activation by dCas9-Tet1

To test whether the dCas9-mediated DNA methylation-editing tools could be used to alter methylation in vivo, we utilized a methylation sensitive reporter mouse previously generated (Figure 7A; Stelzer et al., 2016). In these transgenic mice, a methylation sensitive Snrpn-GFP cassette was inserted into the *Dlk1-Dio3* locus to report the methylation status of its intergenic-differentially methylated region (IG-DMR). As the IG-DMR of this locus acquires paternal methylation during spermatogenesis, the GFP reporter (IG-DMR$^{GFP/Pat}$) is constitutively repressed in heterozygous mice carrying the paternal Snrpn-GFP allele (Stelzer et al., 2016). As shown above, the GFP reporter in the *Dazl* locus was activated by targeted promoter demethylation in mES cells (Figure 1). To assess whether the *Dlk1-Dio3* locus GFP reporter could be activated by dCas9-Tet1 in differentiated cells, we derived adult mouse skin fibroblast cells from the tails of IG-DMR$^{GFP/Pat}$ transgenic mice, which were then transduced by lentiviruses expressing dCas9-Tet1 with *Snrpn* target gRNAs or a scrambled gRNA or a catalytically dead form of Tet1 (dC-dT) with *Snrpn* target gRNAs (Figure 7A). The results in Figures 7B and 7C reveal GFP reporter activation in about 80% of Cherry (gRNA) positive fibroblasts but only when transduced by both dCas9-Tet1 and *Snrpn* gRNAs lentiviruses. FACS analysis of these cells further confirmed this notion (Figures S7A–S7C).

To investigate whether the DNA methylation status can be modified in vivo, we infected three epidermal sites on the ventral side of an IG-DMR$^{GFP/Pat}$ transgenic mouse with the dCas9-Tet1 and *Snrpn* gRNAs (Figure S7D). Cells were sparsely infected with *cherry* expression seen only in some of the hair follicles. dCas9-Tet1 with *Snrpn* gRNAs, but not dCas9-Tet1 with the scrambled gRNA or dC-dT with *Snrpn* gRNAs, was able to activate GFP reporter expression in about 85% infected skin dermal cells in vivo (Figures 7H, S7E, and S7F). In addition, we infected the brain of an IG-DMR$^{GFP/Pat}$ transgenic mouse with lentiviral vectors using a stereotaxic setup and analyzed the effect on targeted DNA methylation in brain slices by confocal microscopy. To eliminate possible inter-individual variability, we injected lentiviral vectors expressing dCas9-Tet1 and *Snrpn* gRNAs, as well as the two negative control vector combinations into different regions of the same brain (Figure 7D). As shown in Figures 7E and 7F, after infection with all three lentiviral combinations, only lentiviral vectors expressing dCas9-Tet1 with *Snrpn* gRNAs, but not vectors expressing dCas9-Tet1 with sc gRNA or dC-dT with *Snrpn* gRNAs, activated the GFP reporter with an activation efficiency of about 70% (Figure 7G).

## DISCUSSION

In this study, we have repurposed the CRISPR/Cas9 system to edit the methylation status of genomic sequences. The catalytically inactive Cas9 protein (dCas9) was fused either to the catalytic domain of Tet1 (dCas9-Tet1) or to Dnmt3a (dCas9-Dnmt3a) to predictably alter the epigenetic state of target sequences. A GFP reporter inserted into the promoter region of the methylated and silenced *Dazl* gene was demethylated and activated when targeted by dCas9-Tet1, whereas the GFP reporter inserted into the promoter region of the active and unmethylated *Gapdh* gene was de novo methylated and silenced when targeted by dCas9-Dnmt3a. When the dCas9-Tet1 was targeted to the inactive *BDNF* promoter IV in post-mitotic neurons, the promoter became demethylated and activated. Importantly, this tool predictably altered the methylation state and activity of regulatory regions: targeted demethylation of the inactive distal enhancer of *MyoD* activated the gene and facilitated muscle cell transdifferentiation and targeted methylation of CTCF anchor sites inhibited CTCF binding and interfered with its function as an insulator between gene loops. Finally, the editing tools can in vivo alter the methylation state of regulatory sequences as injection of the lentiviral vectors of dCas9-Tet1 with target gRNAs into the dermis or brain of transgenic mice demethylated the methylated *Snrpn* promoter in the *Dlk1-Dio3* imprinted locus and activated the methylation-sensing GFP reporter.

(C–E) Doxycycline-inducible dCas9-Dnmt3a mESCs were infected with lentiviruses expressing a scrambled gRNA or CTCF target-1 gRNAs. Cherry-positive cells were FACS sorted, cultured in the presence of Doxycycline, and then harvested for RT-qPCR analysis in (C), for bisulfite-sequencing analysis in (D) and (E). Bars represent mean ± SD of three experimental replicates.

(F) Schematic representation of CTCF target-2 with super-enhancer and Pou5f1 gene in this loop as in (B).

(G–I) The same set of experiments was performed as described in C–E for CTCF target-2, and cells were harvested for RT-qPCR analysis in (G) and for bisulfite sequencing in (H) and (I). Bars represent mean ± SD of three experimental replicates.

See also Figure S6.

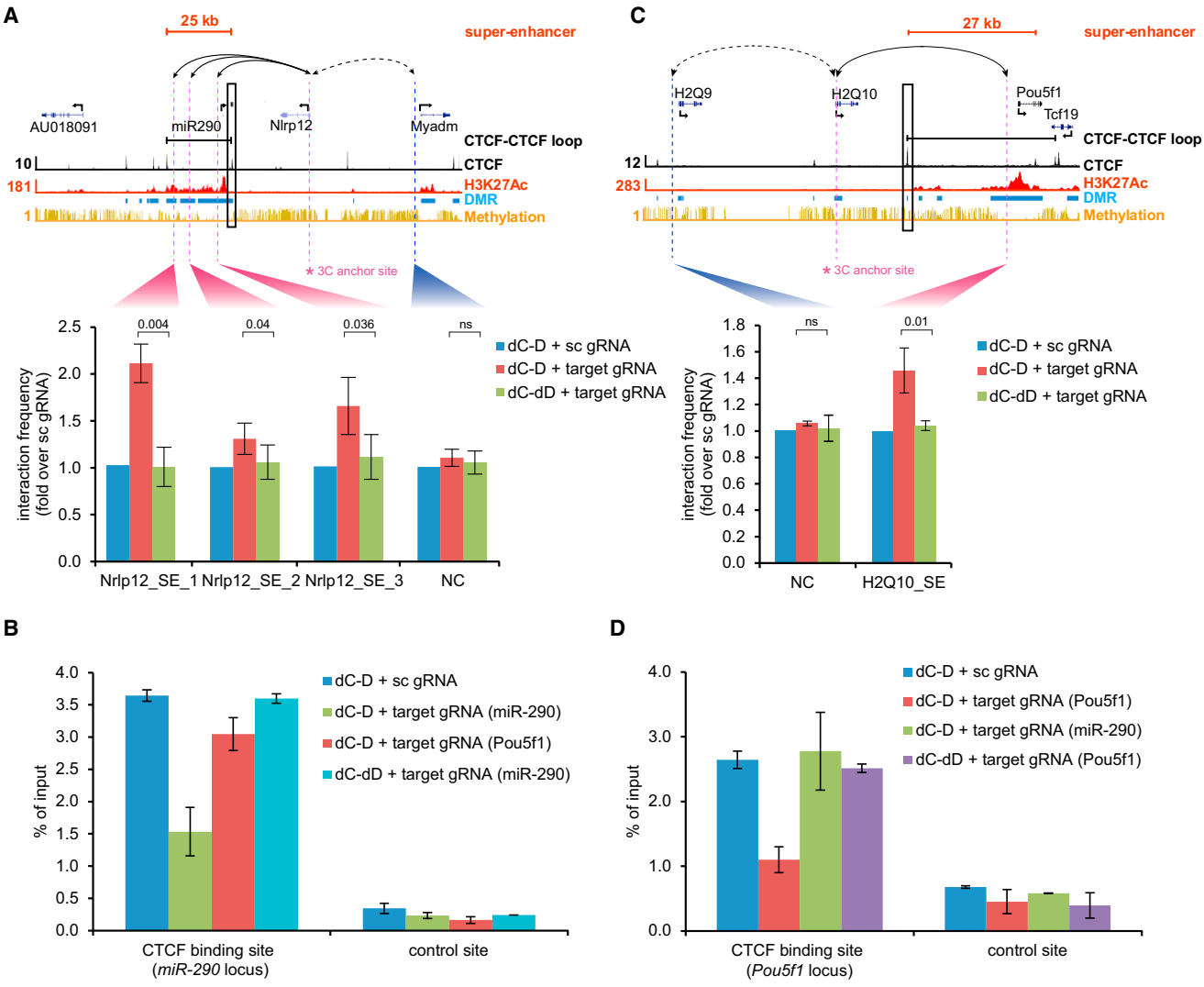


**Figure 6. Targeted Methylation of CTCF Binding Sites to Manipulate CTCF Loops**

(A) Quantitative Chromosome Conformation Capture (3C) analysis of cells described in Figure 5C at the *miR290* locus. The super-enhancer domain is indicated as a red bar. The targeted CTCF site is highlighted with a box. Arrows indicate the chromosomal positions between which the interaction frequency was assayed. Asterisk indicates the 3C anchor site. ChIP-seq binding profiles (reads per million base pair) for CTCF in black and H3K27Ac (super-enhancer) in red, and methylation track in yellow with DMR in blue are also shown. The interaction frequencies between the indicated chromosomal positions and the 3C anchor sites are displayed as a bar chart (mean ± SD) on the bottom panel. qPCRs were run in duplicates, and values are normalized against the mean interaction frequency in cells with a scrambled gRNA. ($p < 0.05$ for all three regions; Student's t test; ns, non-significant; NC, negative control.)

(B) Anti-CTCF ChIP experiment was performed using cells in (A) followed by quantitative PCR analysis. Bars represent mean ± SD of three experimental replicates.

(C) Quantitative Chromosome Conformation Capture (3C) analysis of cells described in Figure 5G at the *Pou5f1* locus as in (A).

(D) Anti-CTCF ChIP experiment was performed using cells in (C) followed by quantitative PCR analysis. Bars represent mean ± SD of three experimental replicates.

Dynamic DNA methylation has been proposed to decode neuronal activities (Sweatt, 2013). For instance, treatment of neurons with KCl has been shown to de-silence promoter IV of *BDNF* and induce BDNF expression associated with demethylation of some methylated CpGs in this promoter region (Chen et al., 2003; Martinowich et al., 2003). When the *BDNF* promoter IV was targeted by dCas9-Tet1, extensive demethylation of methylated CpGs was observed, and BDNF was activated to a similar level as when the cultures were treated with KCl. Because the neurons were post-mitotic, the dCas9-Tet1-mediated demethylation of the promoter sequences was likely the result of active demethylation as has been proposed previously (Wu and Zhang, 2014). Although it is possible that some CpGs in the *BDNF* promoter were 5-fC/5-caC modified after targeting with dCas9-Tet1/gRNA, blocking restoration of 5-fC/5-caC into unmethylated cytosine by inhibition of the BER pathway reduced

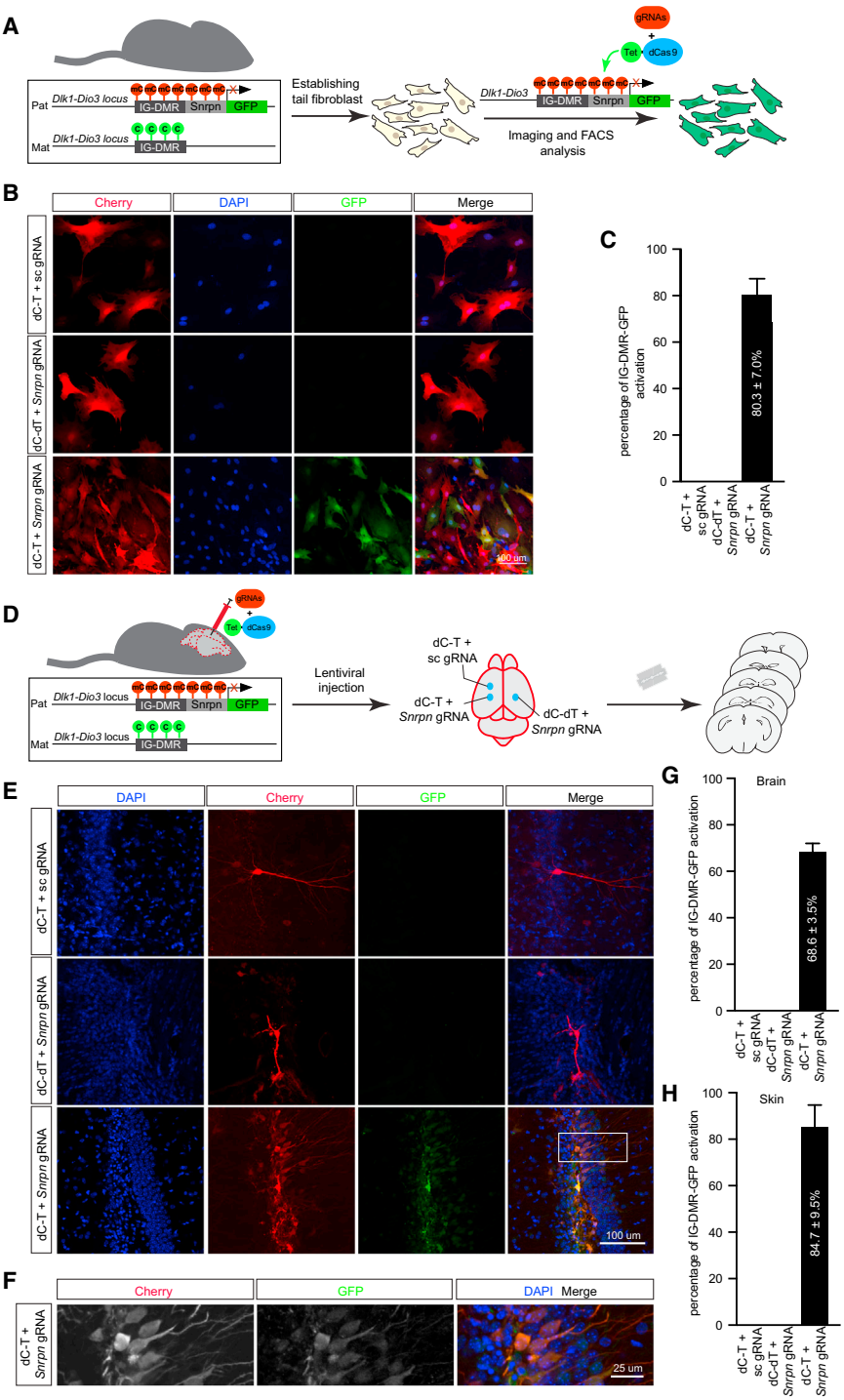


**Figure 7. Targeted Ex Vivo and In Vivo DNA Methylation Editing by dCas9-Tet1 to Activate a Silenced GFP Reporter**

(A) Schematic diagram illustrating the experimental procedure for the ex vivo activation of a silenced GFP reporter in mouse fibroblast cells. Mouse tail fibroblast cells were derived from a genetically modified mouse line carrying a paternal IG-DMR-Snrpn-GFP allele (IG-DMR$^{GFP/Pat}$) in the *Dlk1-Dio3* locus. The *IG-DMR-Snrpn* promoter on the paternal allele is hypermethylated so that the GFP reporter is constitutively silenced. The cultured fibroblast cells were infected with lentiviral vectors expressing dCas9-Tet1 and gRNAs to demethylate the *Snrpn* promoter and activate the GFP reporter.

(B) Representative immunohistochemical images of IG-DMR$^{GFP/Pat}$ fibroblasts infected with lentiviruses expressing dCas9-Tet1 (dC-T) with a sc gRNA, an inactive form of dCas9-Tet1 (dC-dT) with *Snrpn* target gRNA, or dC-T with *Snrpn* target gRNA. Stained in red for Cherry, green for GFP and DAPI for nuclei. Scale bar, 100 μm.

(C) Quantification of the percentage of IG-DMR$^{GFP/Pat}$ mouse fibroblast cells with GFP activation in Cherry (gRNAs) positive cells. Bars represent mean ± SD of three experimental replicates.

(D) Schematic diagram illustrating the experimental procedure for in vivo activation of GFP reporter in the IG-DMR$^{GFP/Pat}$ mouse brain. Lentiviral vectors expressing dC-T and sc gRNA, dC-dT and *Snrpn* target gRNAs, and dC-T and *Snrpn* target gRNAs were delivered with a stereotaxic microinjection approach. Brains were sliced and analyzed by immunohistochemical approaches.

(E) Representative confocal micrographs for the IG-DMR$^{GFP/Pat}$ mouse brains infected with dC-T and sc gRNA, dC-dT and *Snrpn* target gRNAs, and dC-T and *Snrpn* target gRNAs. Only dC-T with the target gRNAs activated the GFP expression. Scale bar, 100 μm.

(F) Confocal micrograph of the boxed area in (E). Stained in red for Cherry, green for GFP and DAPI for nuclei in (E) and (F). Scale bar, 25 μm.

(G and H) Quantification of the percentage of IG-DMR$^{GFP/Pat}$ cells with GFP activation in Cherry (gRNAs) positive cells in the in vivo lentiviral delivery experiment in the brain (G) and in the skin epidemis (H). Bars represent mean ± SD of more than four representative images from two animals. See also Figure S7.

*BDNF* expression, suggesting that demethylation of the *BDNF* promoter IV contributes to the activation of *BDNF*. Importantly, our results establish a causal relationship between the demethylation of *BDNF* promoter IV and gene activation.

The role of DNA methylation as a barrier between cell lineages is consistent with the previous observation that demethylation of DNA in fibroblasts by treatment with 5-Aza can activate MyoD and mediate myotube formation (Constantinides et al., 1977). Targeting of dCas9-Tet1 to the methylated distal enhancer of *MyoD* in fibroblasts induced demethylation of CpGs and resulted in a moderate activation of *MyoD* but failed to generate myoblasts. However, when dCas9-Tet1/gRNA lentiviral transduction was combined with 5-Aza treatment, a significantly enhanced myoblast and myotube formation was observed as compared

to 5-Aza treatment alone. It is possible that demethylation of the additional DMRs in combination with the distal enhancer may be required to induce efficient conversion of fibroblasts to myoblasts.

Recent studies of mammalian chromosome structures reveal that chromatin is organized in topologically associating domains and gene loops mediated by chromatin architecture proteins such as Cohesin and CTCF (Dekker and Mirny, 2016). Emerging data suggest that higher-order chromatin structures confer epigenetic information during development and are frequently altered in cancer (Ji et al., 2016; Narendra et al., 2015). It has been reported that binding of CTCF is inhibited when its recognition sequence is methylated (Bell and Felsenfeld, 2000; Wang et al., 2012). Targeting of dCas9-Dnmt3a to two CTCF binding sites induced de novo methylation of CpGs in these sites and interfered with the insulator function of the protein as evidenced by increased interaction frequencies between insulated super-enhancers in the targeted loop and genes in the neighboring loop causing upregulation of these genes. This suggests that the dCas9-Dnmt3a system is a useful tool to manipulate chromatin structure and to assess its functional significance during development and in disease context.

Our results indicate that dCas9 fused to the epigenetic effectors Tet1 and Dnmt3a represents a powerful toolbox to edit DNA methylation of specific genomic sequences. Comparison of these tools with the TALE-based method showed a higher efficacy and resolution for methylation editing, and dCas9 ChIP-seq followed by bisulfite sequencing of potential off-target binding loci revealed marginal changes in methylation levels, suggesting that high specificity can be achieved with properly designed gRNAs. During the preparation of our manuscript, Vojta et al. also reported that dCas9 fused with Dnmt3a can be used to methylate two human gene promoters (Vojta et al., 2016), and Xu et al. and Choudhury et al. reported that dCas9 fused with Tet1 can be used to demethylate gene promoters (Choudhury et al., 2016; Xu et al., 2016). Therefore, these dCas9-Dnmt3a/Tet1 tools will be useful to gain insight into the functional significance of DNA methylation in diverse biological processes such as gene expression, cell-fate determination, and organization of high-order chromatin structures.

## STAR★METHODS

Detailed methods are provided in the online version of this paper and include the following:

- KEY RESOURCES TABLE
- CONTACT FOR REAGENT AND RESOURCE SHARING
- EXPERIMENTAL MODEL AND SUBJECT DETAILS
  - Mouse lines and breeding strategies
  - Mouse primary cortical neuron culture, EDU labeling, and neural induction
- METHOD DETAILS
  - Plasmid design and construction
  - Cell culture, lentivirus production, and stable cell line generation
  - Viral infection of mice and tissue sample preparation
  - Immunohistochemistry, microscopy, and image analysis
  - FACS analysis
  - Fibroblast-to-myoblast conversion assay
  - Western blot
  - RT-qPCR
  - ChIP assay
  - ChIP-seq data analysis
  - Bisulfite Conversion, PCR and Sequencing
  - Locus-specific TAB-seq
  - Chromosome Conformation Capture (3C) assay
- QUANTIFICATION AND STATISTICAL ANALYSIS
- DATA AND SOFTWARE AVAILABILITY

## SUPPLEMENTAL INFORMATION

Supplemental Information includes seven figures and six tables and can be found with this article online at http://dx.doi.org/10.1016/j.cell.2016.08.056.

## AUTHOR CONTRIBUTIONS

X.S.L. and R.J. conceived the idea for this project. X.S.L. and H.W. designed and conducted the experiments and interpreted the data. X.J. performed ChIP and 3C assay, and Y.S. generated Snrpn-GFP reporter ES cell lines and IG-DMR$^{GFP/Pat}$ reporter mice. S.C., X.W., and J.S. assisted with sequencing analysis. X.S.L., H.W., and R.J. wrote the manuscript with inputs from all the other authors.

## ACKNOWLEDGMENTS

We thank Patti Wisniewski and Colin Zollo for FACS sorting and thank Chuan He, Michael Greenberg, Robert Weinberg, Yupeng He, Joseph Ecker, Klaus Kaestner, Zipeng Fan, Chikdu Shivalila, Dongdong Fu, Johanna Goldmann, Carrie Garrett-Engele, Malkiel Cohen, Robert Plasschaert, Frank Soldner, and Bluma Lesch for reagents, technical assistance, and inputs on the manuscript. This study was supported by NIH grants HD045022, R37-CA084198, HG002668, and GM114864. X.S.L. is supported by a Damon Runyon Cancer Foundation Postdoctoral Fellowship, H.W. is supported by a NARSAD Young Investigator Fellowship, X.W. is supported by a Helen Hay Whitney Foundation Postdoctoral Fellowship, S.C. is supported by the HARMONIA grant no. UMO-2014/14/M/NZ1/00010 from the National Science Centre in Poland, and Y.S. is supported by a Human Frontier Science Program postdoctoral fellowship. R.J. is co-founder of Fate Therapeutics and Fulcrum Therapeutics and an adviser to Stemgent, and R.A.Y. is a founder of Syros Pharmaceuticals.

Received: March 3, 2016
Revised: June 30, 2016
Accepted: August 22, 2016
Published: September 22, 2016

## REFERENCES

Bell, A.C., and Felsenfeld, G. (2000). Methylation of a CTCF-dependent boundary controls imprinted expression of the Igf2 gene. Nature *405*, 482–485.

Bernstein, D.L., Le Lay, J.E., Ruano, E.G., and Kaestner, K.H. (2015). TALE-mediated epigenetic suppression of CDKN2A increases replication in human fibroblasts. J. Clin. Invest. *125*, 1998–2006.

Bird, A. (2002). DNA methylation patterns and epigenetic memory. Genes Dev. *16*, 6–21.

Brambrink, T., Hochedlinger, K., Bell, G., and Jaenisch, R. (2006). ES cells derived from cloned and fertilized blastocysts are transcriptionally and functionally indistinguishable. Proc. Natl. Acad. Sci. USA *103*, 933–938.

Brunk, B.P., Goldhamer, D.J., and Emerson, C.P., Jr. (1996). Regulated demethylation of the myoD distal enhancer during skeletal myogenesis. Dev. Biol. *177*, 490–503.

Chen, W.G., Chang, Q., Lin, Y., Meissner, A., West, A.E., Griffith, E.C., Jaenisch, R., and Greenberg, M.E. (2003). Derepression of BDNF transcription involves calcium-dependent phosphorylation of MeCP2. Science *302*, 885–889.

Chen, B., Gilbert, L.A., Cimini, B.A., Schnitzbauer, J., Zhang, W., Li, G.W., Park, J., Blackburn, E.H., Weissman, J.S., Qi, L.S., and Huang, B. (2013). Dynamic imaging of genomic loci in living human cells by an optimized CRISPR/Cas system. Cell *155*, 1479–1491.

Choudhury, S.R., Cui, Y., Lubecka, K., Stefanska, B., and Irudayaraj, J. (2016). CRISPR-dCas9 mediated TET1 targeting for selective DNA demethylation at BRCA1 promoter. Oncotarget. Published online June 23, 2016. http://dx.doi.org/10.18632/oncotarget.

Cong, L., Ran, F.A., Cox, D., Lin, S., Barretto, R., Habib, N., Hsu, P.D., Wu, X., Jiang, W., Marraffini, L.A., and Zhang, F. (2013). Multiplex genome engineering using CRISPR/Cas systems. Science *339*, 819–823.

Constantinides, P.G., Jones, P.A., and Gevers, W. (1977). Functional striated muscle cells from non-myoblast precursors following 5-azacytidine treatment. Nature *267*, 364–366.

Davis, R.L., Weintraub, H., and Lassar, A.B. (1987). Expression of a single transfected cDNA converts fibroblasts to myoblasts. Cell *51*, 987–1000.

Dawlaty, M.M., Ganz, K., Powell, B.E., Hu, Y.C., Markoulaki, S., Cheng, A.W., Gao, Q., Kim, J., Choi, S.W., Page, D.C., and Jaenisch, R. (2011). Tet1 is dispensable for maintaining pluripotency and its loss is compatible with embryonic and postnatal development. Cell Stem Cell *9*, 166–175.

De Jager, P.L., Srivastava, G., Lunnon, K., Burgess, J., Schalkwyk, L.C., Yu, L., Eaton, M.L., Keenan, B.T., Ernst, J., McCabe, C., et al. (2014). Alzheimer's disease: Early alterations in brain DNA methylation at ANK1, BIN1, RHBDF2 and other loci. Nat. Neurosci. *17*, 1156–1163.

Dekker, J., and Mirny, L. (2016). The 3D Genome as Moderator of Chromosomal Communication. Cell *164*, 1110–1121.

Dixon, J.R., Selvaraj, S., Yue, F., Kim, A., Li, Y., Shen, Y., Hu, M., Liu, J.S., and Ren, B. (2012). Topological domains in mammalian genomes identified by analysis of chromatin interactions. Nature *485*, 376–380.

Dobin, A., Davis, C.A., Schlesinger, F., Drenkow, J., Zaleski, C., Jha, S., Batut, P., Chaisson, M., and Gingeras, T.R. (2013). STAR: Ultrafast universal RNA-seq aligner. Bioinformatics *29*, 15–21.

Dowen, J.M., Fan, Z.P., Hnisz, D., Ren, G., Abraham, B.J., Zhang, L.N., Weintraub, A.S., Schuijers, J., Lee, T.I., Zhao, K., and Young, R.A. (2014). Control of cell identity genes occurs in insulated neighborhoods in mammalian chromosomes. Cell *159*, 374–387.

Ebert, D.H., Gabel, H.W., Robinson, N.D., Kastan, N.R., Hu, L.S., Cohen, S., Navarro, A.J., Lyst, M.J., Ekiert, R., Bird, A.P., and Greenberg, M.E. (2013). Activity-dependent phosphorylation of MeCP2 threonine 308 regulates interaction with NCoR. Nature *499*, 341–345.

Gibcus, J.H., and Dekker, J. (2013). The hierarchy of the 3D genome. Mol. Cell *49*, 773–782.

Gilbert, L.A., Larson, M.H., Morsut, L., Liu, Z., Brar, G.A., Torres, S.E., Stern-Ginossar, N., Brandman, O., Whitehead, E.H., Doudna, J.A., et al. (2013). CRISPR-mediated modular RNA-guided regulation of transcription in eukaryotes. Cell *154*, 442–451.

Gorkin, D.U., Leung, D., and Ren, B. (2014). The 3D genome in transcriptional regulation and pluripotency. Cell Stem Cell *14*, 762–775.

Guo, J.U., Su, Y., Zhong, C., Ming, G.L., and Song, H. (2011). Hydroxylation of 5-methylcytosine by TET1 promotes active DNA demethylation in the adult brain. Cell *145*, 423–434.

Hilton, I.B., D'Ippolito, A.M., Vockley, C.M., Thakore, P.I., Crawford, G.E., Reddy, T.E., and Gersbach, C.A. (2015). Epigenome editing by a CRISPR-Cas9-based acetyltransferase activates genes from promoters and enhancers. Nat. Biotechnol. *33*, 510–517.

Jaenisch, R., and Bird, A. (2003). Epigenetic regulation of gene expression: How the genome integrates intrinsic and environmental signals. Nat. Genet. *33* (*Suppl*), 245–254.

Ji, X., Dadon, D.B., Powell, B.E., Fan, Z.P., Borges-Rivera, D., Shachar, S., Weintraub, A.S., Hnisz, D., Pegoraro, G., Lee, T.I., et al. (2016). 3D Chromosome Regulatory Landscape of Human Pluripotent Cells. Cell Stem Cell *18*, 262–275.

Jinek, M., Chylinski, K., Fonfara, I., Hauer, M., Doudna, J.A., and Charpentier, E. (2012). A programmable dual-RNA-guided DNA endonuclease in adaptive bacterial immunity. Science *337*, 816–821.

Kagey, M.H., Newman, J.J., Bilodeau, S., Zhan, Y., Orlando, D.A., van Berkum, N.L., Ebmeier, C.C., Goossens, J., Rahl, P.B., Levine, S.S., et al. (2010). Mediator and cohesin connect gene expression and chromatin architecture. Nature *467*, 430–435.

Konermann, S., Brigham, M.D., Trevino, A.E., Joung, J., Abudayyeh, O.O., Barcena, C., Hsu, P.D., Habib, N., Gootenberg, J.S., Nishimasu, H., et al. (2015). Genome-scale transcriptional activation by an engineered CRISPR-Cas9 complex. Nature *517*, 583–588.

Landau, D.A., Clement, K., Ziller, M.J., Boyle, P., Fan, J., Gu, H., Stevenson, K., Sougnez, C., Wang, L., Li, S., et al. (2014). Locally disordered methylation forms the basis of intratumor methylome variation in chronic lymphocytic leukemia. Cancer Cell *26*, 813–825.

Lassar, A.B., Paterson, B.M., and Weintraub, H. (1986). Transfection of a DNA locus that mediates the conversion of 10T1/2 fibroblasts to myoblasts. Cell *47*, 649–656.

Lin, Y., Bloodgood, B.L., Hauser, J.L., Lapan, A.D., Koon, A.C., Kim, T.K., Hu, L.S., Malik, A.N., and Greenberg, M.E. (2008). Activity-dependent regulation of inhibitory synapse development by Npas4. Nature *455*, 1198–1204.

Lister, R., Pelizzola, M., Dowen, R.H., Hawkins, R.D., Hon, G., Tonti-Filippini, J., Nery, J.R., Lee, L., Ye, Z., Ngo, Q.M., et al. (2009). Human DNA methylomes at base resolution show widespread epigenomic differences. Nature *462*, 315–322.

Lister, R., Mukamel, E.A., Nery, J.R., Urich, M., Puddifoot, C.A., Johnson, N.D., Lucero, J., Huang, Y., Dwork, A.J., Schultz, M.D., et al. (2013). Global epigenomic reconfiguration during mammalian brain development. Science *341*, 1237905.

Maeder, M.L., Angstman, J.F., Richardson, M.E., Linder, S.J., Cascio, V.M., Tsai, S.Q., Ho, Q.H., Sander, J.D., Reyon, D., Bernstein, B.E., et al. (2013). Targeted DNA demethylation and activation of endogenous genes using programmable TALE-TET1 fusion proteins. Nat. Biotechnol. *31*, 1137–1142.

Mali, P., Yang, L., Esvelt, K.M., Aach, J., Guell, M., DiCarlo, J.E., Norville, J.E., and Church, G.M. (2013). RNA-guided human genome engineering via Cas9. Science *339*, 823–826.

Martinowich, K., Hattori, D., Wu, H., Fouse, S., He, F., Hu, Y., Fan, G., and Sun, Y.E. (2003). DNA methylation-related chromatin remodeling in activity-dependent BDNF gene regulation. Science *302*, 890–893.

Narendra, V., Rocha, P.P., An, D., Raviram, R., Skok, J.A., Mazzoni, E.O., and Reinberg, D. (2015). CTCF establishes discrete functional chromatin domains at the Hox clusters during differentiation. Science *347*, 1017–1021.

Nora, E.P., Lajoie, B.R., Schulz, E.G., Giorgetti, L., Okamoto, I., Servant, N., Piolot, T., van Berkum, N.L., Meisig, J., Sedat, J., et al. (2012). Spatial partitioning of the regulatory landscape of the X-inactivation centre. Nature *485*, 381–385.

Phillips, J.E., and Corces, V.G. (2009). CTCF: Master weaver of the genome. Cell *137*, 1194–1211.

Phillips-Cremins, J.E., Sauria, M.E., Sanyal, A., Gerasimova, T.I., Lajoie, B.R., Bell, J.S., Ong, C.T., Hookway, T.A., Guo, C., Sun, Y., et al. (2013). Architectural protein subclasses shape 3D organization of genomes during lineage commitment. Cell *153*, 1281–1295.

Qi, L.S., Larson, M.H., Gilbert, L.A., Doudna, J.A., Weissman, J.S., Arkin, A.P., and Lim, W.A. (2013). Repurposing CRISPR as an RNA-guided platform for sequence-specific control of gene expression. Cell *152*, 1173–1183.

Robertson, K.D. (2005). DNA methylation and human disease. Nat. Rev. Genet. *6*, 597–610.

Schultz, M.D., He, Y., Whitaker, J.W., Hariharan, M., Mukamel, E.A., Leung, D., Rajagopal, N., Nery, J.R., Urich, M.A., Chen, H., et al. (2015). Human body epigenome maps reveal noncanonical DNA methylation variation. Nature *523*, 212–216.

Smith, Z.D., and Meissner, A. (2013). DNA methylation: Roles in mammalian development. Nat. Rev. Genet. *14*, 204–220.

Stelzer, Y., Shivalila, C.S., Soldner, F., Markoulaki, S., and Jaenisch, R. (2015). Tracing dynamic changes of DNA methylation at single-cell resolution. Cell *163*, 218–229.

Stelzer, Y., Wu, H., Song, Y., Shivalila, C.S., Marloulaki, S., and Jaenisch, R. (2016). Parent-of-origin DNA methylation dynamics during mouse development. Cell Rep. *16*. Published online September 20, 2016. http://dx.doi.org/10.1016/j.celrep.2016.08.066.

Sweatt, J.D. (2013). The emerging field of neuroepigenetics. Neuron *80*, 624–632.

Vojta, A., Dobrinić, P., Tadić, V., Bočkor, L., Korać, P., Julg, B., Klasić, M., and Zoldoš, V. (2016). Repurposing the CRISPR-Cas9 system for targeted DNA methylation. Nucleic Acids Res. *44*, 5615–5628.

Wang, H., Maurano, M.T., Qu, H., Varley, K.E., Gertz, J., Pauli, F., Lee, K., Canfield, T., Weaver, M., Sandstrom, R., et al. (2012). Widespread plasticity in CTCF occupancy linked to DNA methylation. Genome Res. *22*, 1680–1688.

Wilson, M.H., Coates, C.J., and George, A.L., Jr. (2007). PiggyBac transposon-mediated gene transfer in human cells. Mol. Ther. *15*, 139–145.

Wu, H., and Zhang, Y. (2014). Reversing DNA methylation: Mechanisms, genomics, and biological functions. Cell *156*, 45–68.

Wu, H., Luo, J., Yu, H., Rattner, A., Mo, A., Wang, Y., Smallwood, P.M., Erlanger, B., Wheelan, S.J., and Nathans, J. (2014a). Cellular resolution maps of X chromosome inactivation: Implications for neural development, function, and disease. Neuron *81*, 103–119.

Wu, X., Scott, D.A., Kriz, A.J., Chiu, A.C., Hsu, P.D., Dadon, D.B., Cheng, A.W., Trevino, A.E., Konermann, S., Chen, S., et al. (2014b). Genome-wide binding of the CRISPR endonuclease Cas9 in mammalian cells. Nat. Biotechnol. *32*, 670–676.

Xu, W., Yang, H., Liu, Y., Yang, Y., Wang, P., Kim, S.H., Ito, S., Yang, C., Wang, P., Xiao, M.T., et al. (2011). Oncometabolite 2-hydroxyglutarate is a competitive inhibitor of α-ketoglutarate-dependent dioxygenases. Cancer Cell *19*, 17–30.

Xu, X., Tao, Y., Gao, X., Zhang, L., Li, X., Zou, W., Ruan, K., Wang, F., Xu, G.L., and Hu, R. (2016). A CRISPR-based approach for targeted DNA demethylation. Cell Discov. *2*, 16009.

Yu, M., Hon, G.C., Szulwach, K.E., Song, C.X., Zhang, L., Kim, A., Li, X., Dai, Q., Shen, Y., Park, B., et al. (2012). Base-resolution analysis of 5-hydroxymethylcytosine in the mammalian genome. Cell *149*, 1368–1380.

Zhang, Y., Liu, T., Meyer, C.A., Eeckhoute, J., Johnson, D.S., Bernstein, B.E., Nusbaum, C., Myers, R.M., Brown, M., Li, W., and Liu, X.S. (2008). Model-based analysis of ChIP-Seq (MACS). Genome Biol. *9*, R137.

## STAR★METHODS

### KEY RESOURCES TABLE

| REAGENT or RESOURCE | SOURCE | IDENTIFIER |
|---|---|---|
| Antibodies | | |
| Mouse monoclonal anti-Cas9 (IF staining) | Active Motif | Cat#61577 (7A9-3A3) |
| Mouse monoclonal anti-Cas9 (ChIP) | Active Motif | Cat#61757 (8C1-F10) |
| Rabbit polyclonal anti-CTCF | EMD Millipore | Cat#07729; RRID: AB_441965 |
| Chicken polyclonal anti-GFP | Aves Labs | Cat#GFP-1020; RRID: AB_10000240 |
| Rabbit polyclonal anti-BDNF | Abcam | Cat#ab6201; RRID: AB_305367 |
| Chicken polyclonal anti-MAP2 | Encor Biotech | Cat# CPCA-MAP2; RRID: AB_2138173 |
| Mouse monoclonal anti-MAP2 | Sigma-Aldrich | Cat#M2320; RRID: AB_609904 |
| Mouse monoclonal anti-Tuj1 | Biolegend | Cat#MMS-435P |
| Rabbit polyclonal anti-MyoD (C-20) | Santa Cruz Biotechnology | Cat#sc-304; RRID: AB_631992 |
| Mouse monoclonal anti-MHC (MF20) | R&D systems | Cat#MAB4470; RRID: AB_1293549 |
| Chemicals | | |
| 2-Hydroxyglutarate | TRC Toronto Research Chemicals | Cat#H942596 |
| ABT-888 | Selleck | Cat#S1004 |
| 5-Aza-2′-deoxycytidine | Sigma Aldrich | Cat#A3656-5MG |
| Doxycycline hyclate | Sigma Aldrich | Cat#D9891-100G |
| Critical Commercial Assays | | |
| EpiTect Bisulfite Kit | QIAGEN | Cat#59104 |
| TAB-seq kit | Wisegene | Cat#K001 |
| DNeasy Blood & Tissue Kit | QIAGEN | Cat#69504 |
| Zymoclean Gel DNA Recovery Kit | Zymo Research | Cat#D4002 |
| DNA Clean & Concentrator-5 | Zymo Research | Cat#D4013 |
| X-tremeGENE 9 DNA Transfection Reagent | Sigma Aldrich | Cat#6365809001 |
| Xfect mESC Transfection Reagent | Clontech | Cat#631320 |
| Direct-zol RNA Miniprep | Zymo Research | Cat#R2050 |
| SuperScript III First-Strand Synthesis SuperMix | Life Technologies | Cat#18080400 |
| Fast SYBR Green Master Mix | Life Technologies | Cat#4385618 |
| Papain neural tissue dissociation system | Worthington Biochemicals | Cat#LK003150 |
| Click-it EDU labeling kit | Thermo Fischer Scientific | Cat#C10338 |
| Deposited Data | | |
| Raw data files for RNA sequencing | NCBI Gene Expression Omnibus | NCBI GEO: GSE83890 |
| Experimental Models: Organisms/Strains | | |
| Mouse: C57Bl/6J | Jackson Laboratories | RRID: IMSR_JAX:000664 |
| Mouse: B6; Tet1 KO mouse | Dawlaty et al., 2011 | N/A |
| Mouse: B6; Dlk1-Dio3 IG-DMR-Snrpn-GFP | Stelzer et al., 2016 | N/A |
| Experimental Models: Cell Lines | | |
| V6.5 mESC (C57BL/6 × 129S4/SvJae) | Brambrink et al., 2006 | N/A |
| Dazl-Snrpn-GFP V6.5 mESC | Stelzer et al., 2015 | N/A |
| Gapdh-Snrpn-GFP V6.5 mESC | Stelzer et al., 2015 | N/A |
| C3H10T1/2 cell line | Constantinides et al., 1977 | N/A |
| Recombinant DNA | | |
| dCas9-Tet/Dnmt | This paper | N/A |
| pgRNA | This paper | N/A |
| See "Plasmid design and construction" in METHOD DETAILS section | | |

(*Continued on next page*)

*Continued*

| REAGENT or RESOURCE | SOURCE | IDENTIFIER |
|---|---|---|
| Sequence-Based Reagents | | |
| See Tables S2, S3, S4, S5 for primer sequences | This paper | N/A |
| Software and Algorithms | | |
| MACS (ChIP-seq algorithms) | Wu et al., 2014b | http://liulab.dfci.harvard.edu/MACS/ |
| ImageJ (Fiji) | NIH | http://imagej.net/Fiji |

## CONTACT FOR REAGENT AND RESOURCE SHARING

Further information and requests for reagents may be directed to, and will be fulfilled by the corresponding author Rudolf Jaenisch (jaenisch@wi.mit.edu).

## EXPERIMENTAL MODEL AND SUBJECT DETAILS

### Mouse lines and breeding strategies

Tet1 mutant mice were previously generated in our lab (Dawlaty et al., 2011). Tet1 KO mice in the study were maintained in a mixed 129 and C57BL/6 background. To obtain Tet1 KO mice, male and female mice heterozygous for Tet1 were crossed. To obtain wild-type mouse primary cortical neurons, male and female C57BL/6 mice were mated. IG-DMR$^{GFP/Pat}$ methylation reporter mouse line was generated as described (Stelzer et al., 2016). Male mice with IG-DMR$^{GFP/Pat}$ reporter allele were crossed with C57BL/6 females to generate adult offsprings carrying the paternally transmitted allele for in vivo DNA methylation editing analysis. Mice were handled in accordance with institutional guidelines and approved by the Committee on Animal Care (CAC) and Department of Comparative Medicine (DCM) of Massachusetts Institute of Technology.

### Mouse primary cortical neuron culture, EDU labeling, and neural induction

Dissociated E17.5 cortical neuron cultures were generated from wild-type or Tet1 KO mouse embryos as described previously (Ebert et al., 2013). Briefly, E17.5 cortices were dissected in ice-cold 1 X HBSS (GIBCO 14185-052) containing 1 x pen/strep (GIBCO: 15140122), 1 x pyruvate (GIBCO: 11360070) and 30 mM Glucose. Tissues were minced into around 1 $mm^3$ and dissociated with Papain neural tissue dissociation system (Worthington Biochemicals) following the manufacturer's instruction. Cells were resuspended in NM5 media (%5 FBS (Hyclone), 2% B27 supplement (GIBCO 17504044), 1 x pen/strep and 1 x glutamax I (GIBCO 35050-061)). 1 × $10^6$ cells were plated per well of a 6-well plate coated with poly-D-lysine (PDL, Sigma). On DIV2, cells were treated with 2.5 uM AraC overnight (Sigma C-6645) to eliminate the excessive cell division of mitotic astrocytes and neural progenitor cells. Cultures were fed at DIV3 with fresh NM5 media and subsequently membrane depolarized with 50 mM KCl or infected with preferred lentivirus. We started the treatment at the very beginning of the in vitro culture so the step of AP5 and TTX (tetrodotoxin) treatment to silence basal activity in the culture before KCl treatment was omitted. For EDU labeling, primary neuronal culture were treated with EDU at a final concentration of 10 uM for 24 hr followed by Click-it EDU labeling procedure according to the manufacturer's instruction (Thermo Fisher Scientific). Cells were fixed for immunohistochemical analysis, lysed in Trizol to extract total RNA for RT-qPCR or lysed to extract DNA for bisulfite sequencing analysis.

## METHOD DETAILS

### Plasmid design and construction

PCR amplified Tet1 catalytic domain from pJFA344C7 (Addgene plasmid: 49236), Tet1 inactive catalytic domain from MLM3739 (Addgene plasmid: 49959), or Dnmt3a from pcDNA3-hDNMT3A (Addgene plasmid: 35521) were cloned in modified pdCas9 plasmid (Addgene plasmid: 44246) with BamHI and EcoRI sites. Then dCas9-NLS-Tet1 or dCas9-NLS-Dnmt3a were PCR amplified and cloned into FUW vector (Addgene plasmid: 14882) with AscI and EcoRI to package lentiviruses. NLS-dCas9-NLS-Tet1 was cloned by inserting annealed oligos (NLS) into FUW-dCas9-NLS-Tet1 with XbaI and AscI. The gRNA expression plasmids were cloned by inserting annealed oligos into modified pgRNA plasmid (Addgene plasmid: 44248) with AarI site. The PiaggyBac-dCas9-Tet1 and -dCas9-Dnmt3a were cloned by ligation of PCR-amplified dCas9-NLS-Tet1 or dCas9-NLS-Dnmt3a from FUW constructs with modified PiggyBac transposon vector (Wilson et al., 2007) with NheI and EcoRI. All constructs were sequenced before transfection. Primer information for gRNA design and construction is listed in Table S2. Related plasmids have been deposited into Addgene plasmid database. TALE-Dnmt3a construct targeting *p16* locus is a gift from Dr. Klaus Kaestner, and TALE-Tet1 targeting *RHOXF2* locus is from Addgene (Plasmid #49943). Full-length protein sequences of dCas9-Dnmt3a and dCas9-Tet1CD and their mutants are listed in Table S6.

### Cell culture, lentivirus production, and stable cell line generation

Mouse embryonic stem cells (mESCs) were cultured on irradiated mouse embryonic fibroblasts (MEFs) with standard ESCs medium: (500 ml) DMEM supplemented with 10% FBS (Hyclone), 10 ug recombinant leukemia inhibitory factor (LIF), 0.1 mM β-mercaptoethanol (Sigma-Aldrich), penicillin/streptomycin, 1 mM L-glutamine, and 1% nonessential amino acids (all from Invitrogen). C3H10T1/2 cells were cultured in standard DEME medium with 10% FBS. Lentiviruses expressing dCas9-Tet1, dCas9-Dnmt3a, and gRNAs were produced by transfecting HEK293T cells with FUW constructs or pgRNA constructs together with standard packaging vectors (pCMV-dR8.74 and pCMV-VSVG) followed by ultra-centrifugation-based concentration. Virus titer (T) was calculated based on the infection efficiency for 293T cells, where T = (P*N) / (V), T = titer (TU/ul), p = % of infection positive cells according to the fluorescence marker, N = number of cells at the time of transduction, V = total volume of virus used. Note TU stands for transduction unit. To generate stable cell lines with integrated Doxycycline-inducible dCas9-Tet1 or dCas9-Dnmt3a transgenes, PiggyBac-dCas9-Tet1 or -dCas9-Dnmt3a construct, with a helper plasmid expressing transposase, were transfected into C3H10T1/2 cell using X-tremeGENE 9 transfection reagent (Roche) or into mESCs cells using Xfect transfection reagent (Clontech), according to the provider's protocol. Stably integrated cells were selected with G418 (400 ug/ml) for 10 days. Adult mouse fibroblasts were derived from tails of IG-DMR$^{GFP/Pat}$ reporter mice. Briefly, ~2 cm-long mouse tail was obtained from 3 month old mouse carrying paternally transmitted IG-DMR-Snrpn-GFP methylation reporter, and sterilized by 70% EtOH. ~2 mm x 2 mm minced tail pieces were digested with 5 ml of 1mg/ml Collagenase IV at 37°C for 90 min in a 15 ml Falcon tube. 5 ml MEF medium were added into the tube to terminate the digestion. Dissociated cells were extruded through a 40 um cell strainer with gentle grind using a syringe plug. Cells were then collected and cultured for viral infection. Cells were analyzed 3 days post-infection in this study.

### Viral infection of mice and tissue sample preparation

Mice were infected with appropriate lentiviral cocktails in accordance with institutional guidelines and approved by the Committee on Animal Care (CAC) and Department of Comparative Medicine (DCM) of Massachusetts Institute of Technology. Specifically, to infect mouse skin, lentiviruses expressing dCas9-Tet1 with sc gRNA, an inactive mutant of dC-dT with target gRNAs, and dCas9-Tet1 with target gRNAs were delivered by Hamilton syringe into multiple dermal sites on the ventral side of the deeply anesthetized mouse carrying the Paternal IG-DMR$^{GFP}$ reporter allele (Figure S7D). To infect mouse brain, various lentiviral mixtures were delivered by stereotaxic setup (Leica BIOSYSTEMS, BenchMark Digital Stereotaxic with Manual Fine Drive) into the following locations (relative to the Franklin and Paxinos mouse brain atlas) of the deeply anesthetized mouse carrying the paternal IG-DMR$^{GFP/Pat}$ reporter allele (Figure 7D): dCas9-Tet1 with sc gRNA (A-P 0.70mm, M-L 1.50mm, D-V 1.50mm), an inactive mutant of dC-dT with *Snrpn* gRNAs (A-P −1.90mm, M-L −1.50mm, D-V 1.50mm), and dCas9-Tet1 with *Snrpn* gRNAs (A-P −1.90mm, M-L 1.50mm, D-V 1.50mm). The titers for dC-T/dC-dT and gRNA lentiviruses are $1.2 \times 10^4$ TU/ul and $1.2 \times 10^5$ TU/ul respectively. Mice were sacrificed 3 days after infection. The animals were fixed by transcardial perfusion with 4% paraformaldehyde (PFA)/PBS. Fixed skin pads and brain samples were dissected and post fixed with 4% paraformaldehyde (PFA)/PBS overnight at 4°C. The brain samples were sectioned with a vibratome (Leica VT1100) at 150 um thickness and the skin samples were sectioned with a cryostat (Leica) at 10 um thickness followed by immunohistochemical analysis. For vibratome sectioning, tissues were embedded in 3% agarose gel. For cryosectioning, tissues were equilibrated in 30% sucrose/PBS prior to embedding in Optimal Cutting Temperature (OCT) compound.

### Immunohistochemistry, microscopy, and image analysis

Neurons, HEK293T cells, mouse ES cells and C3H10T1/2 cells were fixed with 4% paraformaldehyde (PFA) for 10 min at room temperature. Cells were permeablized with PBST (1 x PBS solution with 0.1% Triton X-100) before blocking with 10% Normal Donkey Serum (NDS) in PBST. Cells were then incubated with appropriately diluted primary antibodies in PBST with 5% NDS for 1 hr at room temperature or 12 hr at 4°C, washed with PBST for 3 times at room temperature and then incubated with desired secondary antibodies in TBST with 5% NDS and DAPI to counter stain the nuclei. Cells were washed 3 times with PBST before mounted onto slides with Fluoromount G (SouthernBiotech). Immunostaining procedures for tissue sections were previously described (Wu et al., 2014a). Briefly, sections were permeablized with PBST (1 x PBS solution with 0.5% Triton X-100) for 1 hr at RT before blocking with 10% Normal Donkey Serum (NDS) in PBST. Slices were then incubated with desired primary antibodies in PBST with 5% NDS for 24 hr at 4°C, washed with PBST for 3 times at room temperature and then incubated with secondary antibodies in TBST with 5% NDS and DAPI to counter stain the nuclei. Sections were washed 3 times with PBST before slide mounting. The following antibodies were used in this study: Chicken anti-GFP (1:1000, Aves Labs), Mouse anti-Cas9 (7A9, 1:1000, Active Motif), Rabbit anti-BDNF (1:1000, Abcam), Chicken anti-MAP2 (1:1000, Encor Biotech), Mouse anti-MAP2 (1:1000, Sigma-Aldrich), Mouse anti-Tuj1 (1:1000, Biolegend), Rabbit anti-MyoD (C-20, 1:1000, Santa Cruz Biotechnology), Mouse anti-MHC (MF20, 1:1000, R&D systems). Images were captured on a Zeiss LSM710 confocal microscope and processed with Zen software, ImageJ/Fiji, and Adobe Photoshop. For imaging based quantification, unless otherwise specified, 3-5 representative images were quantified and data were plotted as mean ± SD with Excel or Graphpad.

### FACS analysis

To assess the proportion of GFP and/or Cherry positive cells after treatment, the treated cells were dissociated with trypsin and single-cell suspensions were prepared in growth medium subject to a BD FACSAria cell sorter according to the manufacture's protocol at the Whitehead Institute Flow Cytometry Core. Data were analyzed with FlowJo software.

### Fibroblast-to-myoblast conversion assay

Myoblast conversion assay was described previously (Constantinides et al., 1977). Briefly, C3H10T1/2 mouse embryonic fibroblast cells were plated as 1 × $10^4$ cells per well in 6-well plate, and then infected with lentiviruses expressing dCas9-Tet1 and target gRNAs. 24 hr post infection, cells were treated with vehicle control (HEPES buffer) or 5-Azacytidine (1 uM) for 24 hr, and harvested at different time points for subsequently analysis. DMRs upstream of mouse *MyoD* gene were defined based on human/mouse genome homology (Schultz et al., 2015).

### Western blot

HEK293T cells were transfected with various constructs by X-tremeGENE 9 reagent following manufacturer's protocol. 2-day post transfection, cells were lysed by RIPA buffer with proteinase inhibitor (Invitrogen), and subject to standard immunoblotting analysis. Mouse anti-Cas9 (1:1000, Active Motif) and mouse α-Tubulin (1:1000, Sigma) antibodies were used.

### RT-qPCR

Cells were harvested using Trizol followed by Direct-zol (Zymo Research), according to manufacturer's instructions. RNA was converted to cDNA using First-strand cDNA synthesis (Invitrogen SuperScript III). Quantitative PCR reactions were prepared with SYBR Green (Invitrogen), and performed in 7900HT Fast ABI instrument. Primer information for RT-qPCR is listed in Table S3.

### ChIP assay

ChIP experiment was performed as previously described (Dowen et al., 2014). Briefly, cells were cross-linked by 1% formaldehyde in the medium for 10 min in room temperature, and then quenched by adding 0.125 M Glycine for 5 min. Collected cells were washed with PBS twice, and then re-suspended in 3.5 ml of sonication buffer. Sonication was performed for 10 cycles with 0.5 min pulse on and 1 min rest, and 24 W in ice-water mixture. Then cell lysate was spun down with 14,000 x rpm for 10 min at 4°C. 50 ul of supernatant was saved as input for gDNA. 10 ul of anti-CTCF antibody (EMD Millipore: 07729) or anti-Cas9 antibody (Active Motif) was added and incubate overnight at 4°C. 50 ul protein G dynabeads was added into antibody-cell lysate mixture and incubate overnight at 4°C. Then beads were washed with sonication buffer, sonication buffer with high salt (500 mM NaCl), LiCl wash buffer, and TE buffer. Bound protein-DNA complex was eluted from beads by incubation in a 65°C oven for 15 min, and then reverse cross-linked under 65°C overnight. The bound DNA was purified with QIAGEN QIAquick PCR Purification Kit, and then subject to qPCR analysis or sequencing.

### ChIP-seq data analysis

Sequencing data was analyzed with a previously reported method (Wu et al., 2014b). Reads are de-multiplexed and the first 25 bases are mapped to mouse genome (mm10) using STAR (Dobin et al., 2013), requiring unique mapping allowing one mismatch. Mapped reads are collapsed and the same number of reads (about 15 million) are randomly sampled from each sample to match sequencing depth. Peaks are called using MACS (Zhang et al., 2008) with default settings. For each sample, the other five samples are each used as a control and only peaks called over all five controls are defined as candidate peaks. Candidate peaks are filtered by fold of enrichment over background and the threshold is chosen such that no peaks pass this threshold in the four control samples (input, mock IP, dCas9 alone, and scrambled gRNA). Note that six candidate peaks in input mapped to 45S rRNA and mitochondria DNA are excluded from the analysis. Raw data is available in the following link: http://www.ncbi.nlm.nih.gov/geo/query/acc.cgi?token=ktohskmgnhudhud&acc=GSE83890

### Bisulfite Conversion, PCR and Sequencing

Bisulfite conversion of DNA was established using the EpiTect Bisulfite Kit (QIAGEN) following the manufacturer's instructions. The resulting modified DNA was amplified by first round of nested PCR, following a second round using loci specific PCR primers (Table S3). The first round of nested PCR was done as follows: 94°C for 4 min; 55°C for 2 min; 72°C for 2 min; Repeat steps 1-3 1 X; 94°C for 1 min; 55°C for 2 min; 72°C for 2 min; Repeat steps 5-7 35X; 72°C for 5 min; Hold 12°C. The second round of PCR was as follows: 95°C for 4 min; 94°C for 1 min; 55°C for 2 min; 72°C for 2 min; Repeat steps 2-4 35 X; 72°C for 5 min; Hold 12°C. The resulting amplified products were gel-purified, sub-cloned into a pCR2.1-TOPO-TA cloning vector (Life technologies), and sequenced. Primer information for bisulfite sequencing is listed in Table S4.

### Locus-specific TAB-seq

TAB-Seq was performed as described previously (Yu et al., 2012). Briefly, 1 ug of genomic DNA from treated mouse cortical neuron was glucosylated in a solution containing 50 mM HEPES buffer (pH 8.0), 25 mM MgCl2, 100 ng/ml model DNA, 200 mM UDP-Glc, and 1 mM bGT at 37C for 1 hr. After the reaction, the DNA was column purified. The oxidation reactions were performed in a solution containing 50 mM HEPES buffer (pH 8.0), 100 mM ammonium iron (II) sulfate, 1 mM a-ketoglutarate, 2 mM ascorbic acid, 2.5 mM DTT, 100 mM NaCl, 1.2 mM ATP, 15 ng/ml glucosylated DNA, and 3 mM recombinant mTet1. The reactions were incubated at 37C for 1 hr. After proteinase K treatment, the DNA was column purified and then applied to EpiTect Bisulfite Kit (QIAGEN) following the supplier's instruction. The resulting modified DNA was amplified by first round of nested PCR, following a second round using loci specific PCR primers (Table S3). The resulting amplified products were gel-purified, sub-cloned into a pJET cloning vector (Life technologies), and sequenced. Primer information for bisulfite sequencing is listed in Table S4.

### Chromosome Conformation Capture (3C) assay

$5 \times 10^6$ mESCs were fixed with 1% formaldehyde for 20 min at room temperature, and the reaction was quenched by 0.125 M glycine for 5 min at room temperature. Cross-linked cells were collected and washed with 1 ml ice cold PBS. Cell pellet was re-suspended with 550 μl lysis buffer (10 mM Tris-HCl with pH 8.0, 10 mM NaCl, and 0.2% IGEPAL CA630 with proteinase inhibitor), and incubated on ice for 20 min. Cell pellet was then washed twice with 1 × NEB buffer 2 (NEB, B7002S), then incubated with 50 ìl 0.5% SDS for 10 min at 62°C. After heating, 145 ìl $H_2O$ and 25 μl 10% Triton X-100 were added into the mixture and incubate for 15 min at 37°C. 25 μl 10 × NEB buffer 2 and 100 U BglII (NEB, R0144S) were added to digest chromatin over night at 37°C. The digest reaction was inactivated by incubation for 20 min at 62°C. Then 713 μl H2O, 120 μl 10 × T4 DNA ligase buffer (NEB, B0202), 100 μl 10% Triton X-100, 12 μl 10 mg/ml BSA, and 5 μl T4 DNA ligase (NEB, M0202) were added and incubated for 22 hr at 16°C. The chromatin was reverse cross-linked, and DNA was purified by phenol:chloroform:isoamyl alcohol (Sigma, P3803) extraction. The 3C interactions at the *miR290* and *Pou5f1* loci (Figures 6A and 6C) were analyzed by quantitative real-time PCR using custom Taqman probes. The amount of DNA in the qPCR reactions was normalized across 3C libraries using a custom Taqman probe directed against the *Actb* locus. Primer and probe sequences are listed in Table S5.

## QUANTIFICATION AND STATISTICAL ANALYSIS

Statistical parameters including the exact value of n, the definition of center, dispersion, and precision measures (mean ± SEM) and statistical significance are reported in the Figures and the Figure Legends. Data is judged to be statistically significant when $p < 0.05$ by two-tailed Student's T-Test or 2-way ANOVA, where appropriate.

## DATA AND SOFTWARE AVAILABILITY

The accession number for the raw data files for the ChIP-seq analysis is NCBI Gene Expression Omnibus: GSE83890.

Cell

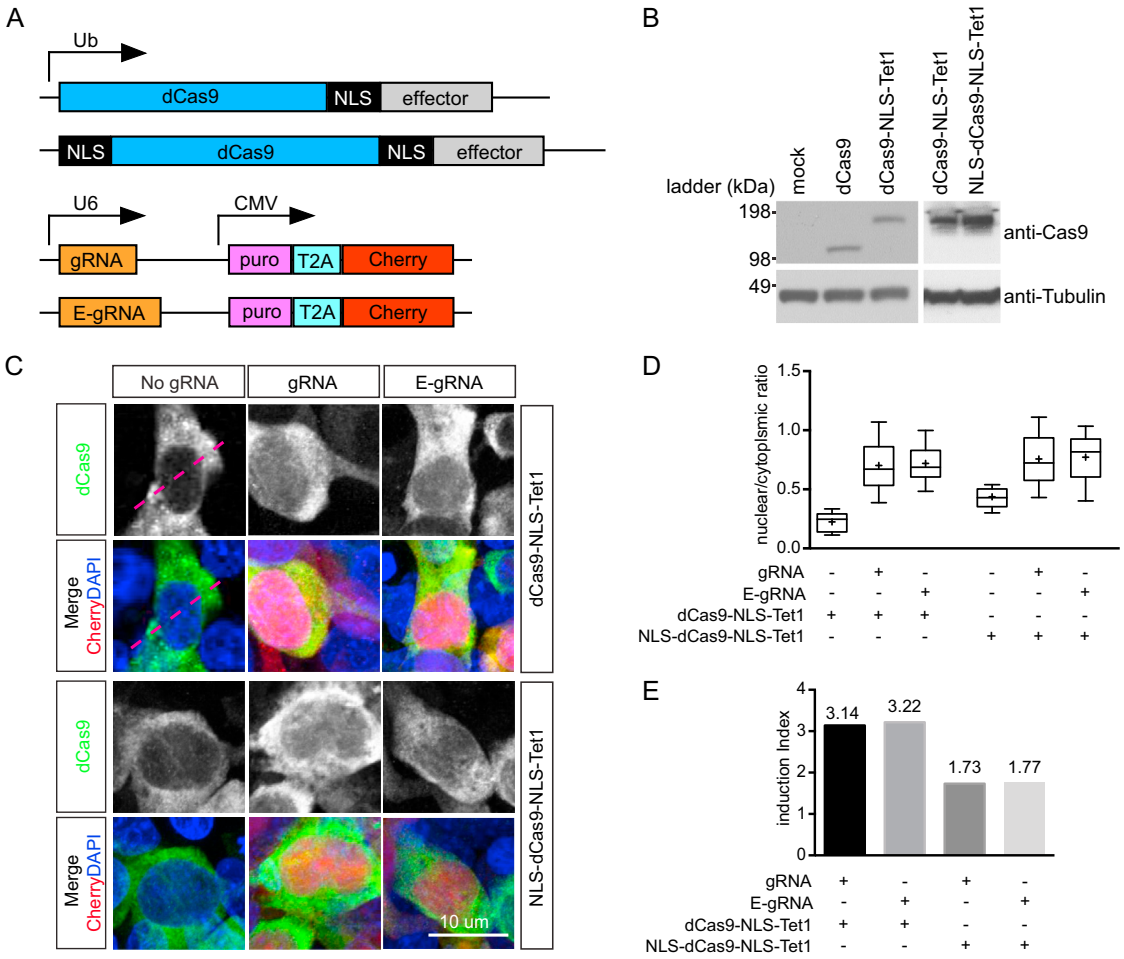


**Figure S1. A Modified CRISPR System for Editing 5-Cytosine DNA Methylation in the Mammalian Genome, Related to Figure 1**

(A) Design of dCas9-effector constructs with nuclear localization signal (NLS) located at different positions, and guide RNA (gRNA) or enhanced guide RNA (E-gRNA) with CMV-driven puro-T2A-Cherry cassette. Ub: human Ubiquitin C promoter.

(B) Expression of dCas-NLS-Tet1 and NLS-dCas9-NLS-Tet1 was analyzed by immunoblotting with anti-Cas9 antibody after transfection with these constructs in HEK293T cells for 2 days. α-tubulin was used as a loading control.

(C) Comparison of the cellular localization of dCas9-NLS-Tet1 and NLS-dCas9-NLS-Tet1 in HEK293T cells with or without co-expression of a gRNA or E-gNRA targeting the same position in the *MyoD* locus. In the absence of sgRNAs, dCas9-NLS-Tet1 is predominantly excluded from the nuclear compartment, and NLS-dCas9-NLS-Tet1 shows weak nuclear localization in transfected HEK293T cells. Co-expression of either gRNA or E-gRNA induced cytoplasm-to-nucleus translocation of these two proteins. Stained in green for dCas9, red for Cherry and blue for DAPI in the merged images. The red dashed lines in the first two panels indicate the cross section of the images for GFP intensity quantification. Scale bar: 10 um.

(D) Quantification of the nuclear-cytoplasmic ratio of dCas9-NLS-Tet1 and NLS-dCas9-NLS-Tet1 in HEK293T cells in the absence or presence of a gRNA, or an E-gNRA in a Box and Whiskers plot. Average dCas9 intensity of cytoplasmic and nuclear domain along a cross-sectional line as illustrated in C was used for the quantification. "+" denotes mean value of the 20 data points in each group; the boxes indicate the extreme data points (top and bottom bars), the 25%–75% interval (box), and the median (central line).

(E) Quantification of induction index (defined as the nuclear-cytoplasmic ratio with sgRNA normalized to that without sgRNA) for dCas9-NLS-Tet1 and NLS-dCas9-NLS-Tet1. gRNA and E-gRNA induced 3.17 and 3.22 folds of nuclear localization for dCas9-NLS-Tet1, and 1.73 and 1.77 folds for NLS-dCas9-NLS-Tet1, respectively. We reasoned that the combination with the highest induction index would result in the best signal-to-noise ratio for targeted DNA methylation editing.

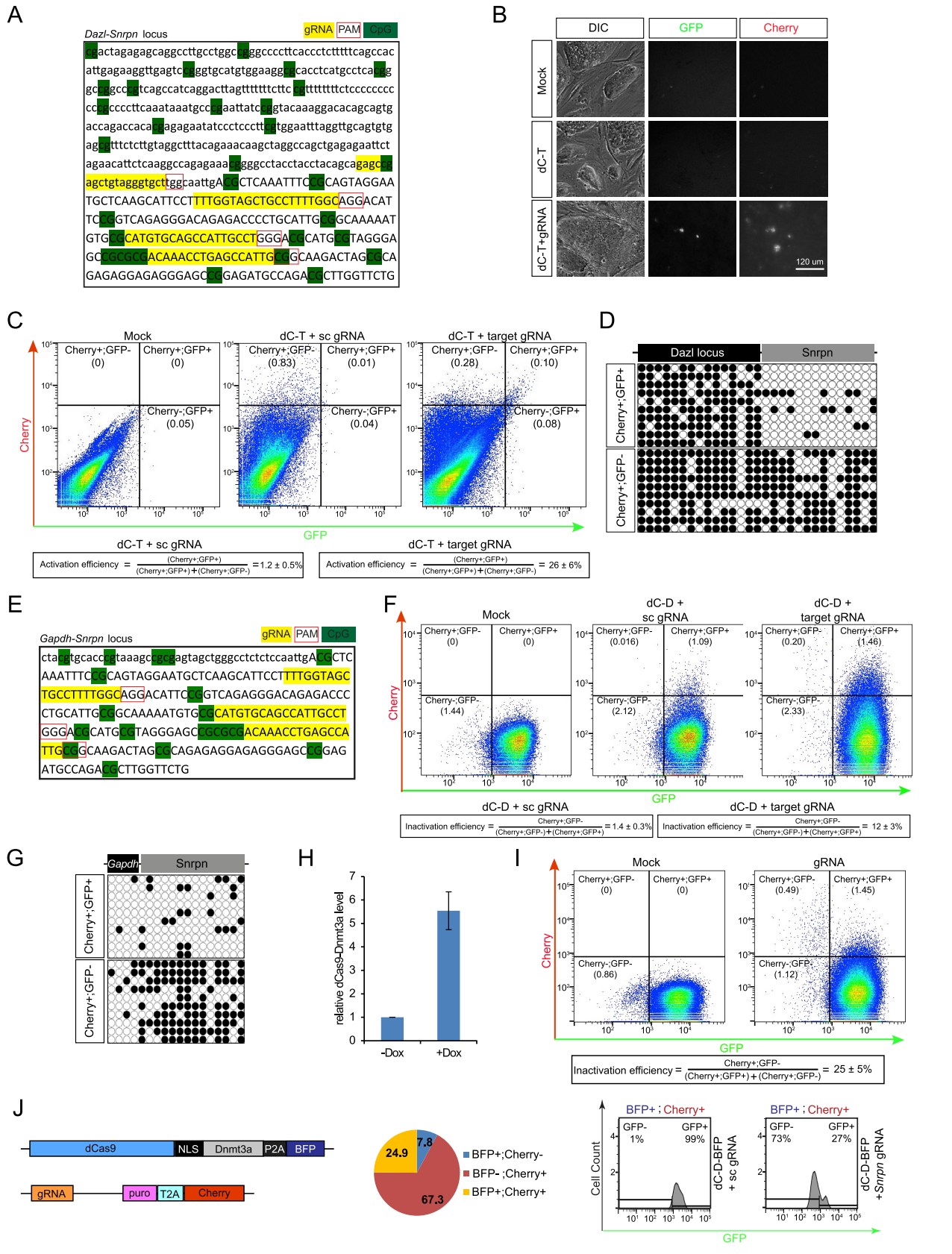


(legend on next page)

**Figure S2. Targeted Promoter Methylation Editing to Activate Dazle-Snrpn-GFP Reporter by dCas9-Tet1 and Repress Gapdh-Snrpn-GFP Reporter by dCas9-Dnmt3a, Related to Figure 2**

(A) Genomic sequence of the *Dazl-Snrpn* locus with gRNA sequences labeled in yellow and CpGs in green. PAM for each gRNA is highlighted by a red box. The *Dazl* sequence is in lower case, and the *Snrpn* sequence is in upper case.

(B) Fluorescence images of Dazl-Snrpn-GFP mESCs infected with lentiviruses expressing dCas9-Tet1 (dC-T) with or without target gRNAs for the *Snrpn* promoter for 3 days. Scale bar: 120 um.

(C) Flow cytometric analysis of Dazl-Snrpn-GFP mESCs 3-day after infection with lentiviruses to express dCas9-Tet1 (dC-T) with a scrambled gRNA or 4 gRNAs targeting the *Snrpn* promoter region. Activation efficiency was calculated by the listed equation and shown as the mean percentages of Cherry and GFP double positive cells ± SD of two biological replicates.

(D) Bisulfite sequencing of the *Dazl-Snrpn* region in Cherry+;GFP+ or Cherry+;GFP- cell populations after FACS sorting of Dazl-Snrpn mouse ES cells infected with lentiviruses expressing dC-T and *Snrpn* gRNAs.

(E) Genomic sequence of the *Gapdh-Snrpn* locus with gRNA sequences labeled in yellow and CpGs in green. PAM for each gRNA is highlighted by a red box. The *Gapdh* sequence is in lower case, and the *Snrpn* sequence is in upper case.

(F) Flow cytometric analysis of Gapdh-Snrpn-GFP mESCs at 3-days after infection with lentiviruses to express dCas9-Dnmt3a (dC-D) and 3 gRNAs targeting the *Snrpn* promoter region. Inactivation efficiency was calculated by the listed equation and shown as the mean percentage of Cherry positive and GFP negative cells ± SD of two biological replicates.

(G) Bisulfite sequencing of the *Gapdh-Snrpn* region in Cherry+;GFP+ or Cherry+;GFP- cell populations after FACS sorting of Gapdh-Snrpn mouse ES cells infected with lentiviruses expressing dC-D and *Snrpn* gRNAs.

(H) mESCs with stably integrated Doxycycline-inducible dCas9-Dnmt3a cassette were analyzed by RT-qPCR after Doxycycline (2 ug/ml) treatment for 48 hr. Bars represent mean ± SD of three experimental replicates.

(I) Flow cytometric analysis of Gapdh-Snrpn-GFP mESCs with Doxycycline-inducible dCas9-Dnmt3a after 3-day infection with lentiviruses expressing the same 3 gRNAs as in F in the presence of Doxycycline (2 ug/ml). Inactivation efficiency was calculated as shown at the bottom and is expressed as the mean percentage of Cherry positive and GFP negative cells ± SD of two biological replicates.

(J) Left panel: Schematic diagram of dCas9-Dnmt3a-P2A-BFP construct and gRNA-Cherry constructs. Middle panel: Percentages of BFP-positive only, Cherry-positive only, and double positive cell populations by FACS analysis of Gapdh-Snrpn-GFP mESCs after infection with lentiviruses expressing dCas9-Dnmt3a-P2A-BFP and *Snrpn* gRNAs. Right panel: FACS analysis of the percentages of GFP- or GFP+ cells within BFP+;Cherry+ cell population.

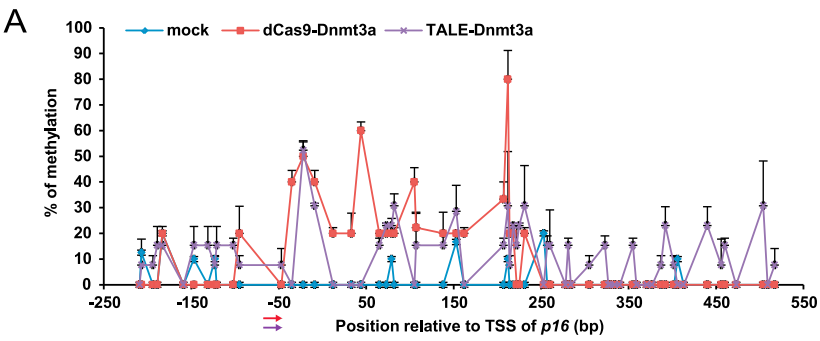


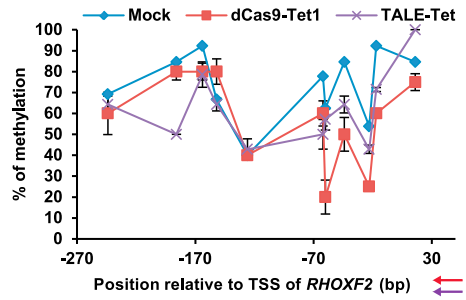


C

| | No. of colonies sequenced | Effective range (resolution) | Average Efficacy | Specificity |
|---|---|---|---|---|
| dCas9-Dnmt3a | 34 | 320 bp | 25% | high |
| TALE-Dnmt3a | 31 | 650 bp | 13% | N/A |
| | | | | |
| dCas9-Tet1 | 34 | 150 bp | -28% | high |
| TALE-Tet1 | 38 | 200 bp | -14% | N/A |

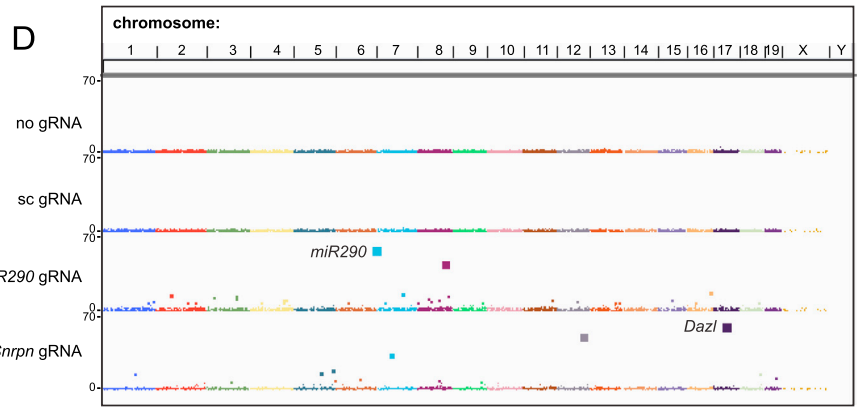



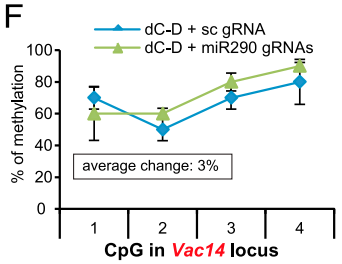


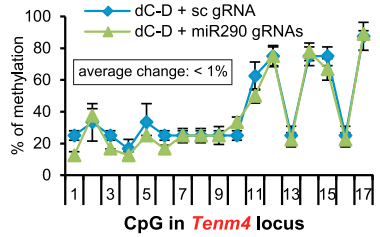


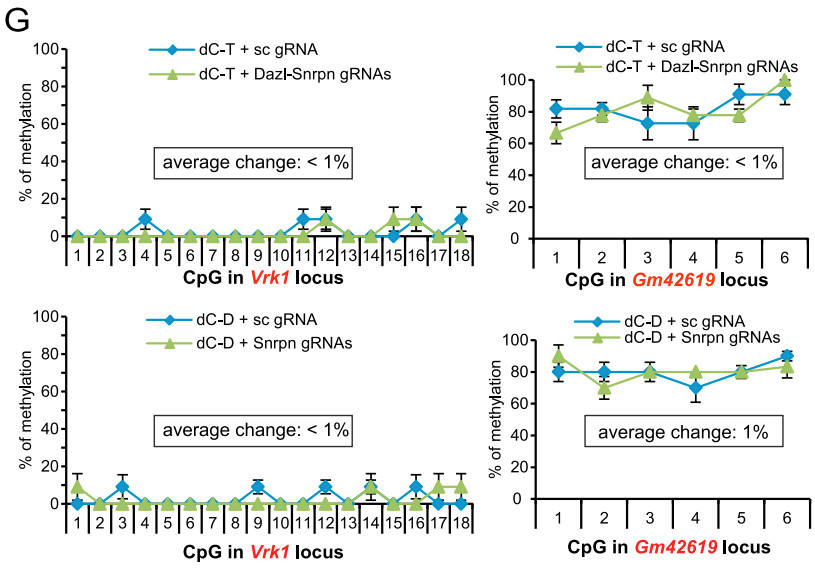


(legend on next page)

**Figure S3. Comparison of TALE- and dCas9-Based Methylation Editing, Related to Figure 2**

(A) HeLa cells were transfected with dCas9-Dnmt3a and one *p16* target gRNA (cherry) or TALE-Dnmt3a-GFP. Transfection positive cell populations (cherry+) or (GFP+) were FACS sorted 48 hr post-transfection. Methylation levels of each individual CpG in the *p16* promoter region were analyzed by bisulfite sequencing. Shown is the mean percentage ± SD of two biological replicates with a total of 34 single colonies sequenced for dCas9-Dnmt3a and 31 single colonies sequenced for TALE-Dnmt3a. Red arrow indicates the position of *p16* target gRNA, and purple arrow indicates the binding site for TALE-Dnmt3a.

(B) HEK293T cells were co-transfected with dCas9-Tet1 and one *RHOXF2* target gRNA (with *puro* cassette) or TALE-Tet1 with a *puro* cassette expressing plasmid. Puromycin (2 ug/ml) was added to the culture medium to select for transfection positive cells. Cells were harvested after 2-day selection for analysis of methylation levels for individual CpGs in the *RHOXF2* promoter region by bisulfite sequencing. Shown is the mean percentage ± SD of two biological replicates with a total of 34 single colonies sequenced for dCas9-Tet1 and 38 single colonies sequenced for TALE-Tet1. Red arrow indicates the position of *RHOXF2* target gRNA, and purple arrow indicates the binding site for TALE-Dnmt3a.

(C) Summary of methylation level analysis in A and B. The effective range was determined by the distance of CpGs that were significantly edited by dCas9-Dnmt3a/Tet1 (change of methylation greater than 10%) from the site of gRNA targeting. The resolution is defined as the effective range of dCas9-Dnmt3a/Tet1 with one single gRNA, and better resolution is referred to the shorter effective range of dCas9-Dnmt3a/Tet1 which will allow for more precise editing of DNA methylation.

(D) Dox-inducible dCas9-Dnmt3a expression mouse ES cells described in Figure S2H were infected with a scrambled gRNA or gRNAs targeting the *miR290* locus or *Dazl-Snrpn* locus. FACS sorted Cherry-positive cells were cultured with Dox (2 ug/ml) for 3 days. Then these cells were harvested for anti-dCas9 ChIP-seq analysis. Peaks were called with the pairwise peak calling procedure described previously (Wu et al., 2014b), and presented in a Manhattan plot depicting genome-wide ChIP-seq peaks. All peaks with $p < 0.001$ are shown. Each dot represents a peak, with the x axis showing genomic location and y axis showing the peak summit height output by Model-based Analysis of ChIP-Seq (MACS) (Zhang et al., 2008). The size of each dot is proportional to its y axis value, and individual chromosome is colored differently for visualization.

(E) ChIP-seq peaks at the targeted loci (*miR290* or *Dazl-Snrpn*) with the highest level of signal and at two off-target loci with the second and third highest signals (*Vac14* and *Tenm4* loci for *miR290* gRNAs; *Vrk1* and *Gm42619* loci for *Dazl-Snrpn* gRNAs) are illustrated with the nearby genes listed below. Note that the 4 *Dazl-Snrpn* gRNAs recognize the promoter sequences of *Dazl* and *Snrpn* as described in Figure S2A, so the peaks for this group of gRNAs were mapped to both loci.

(F) Genomic DNA from cells used in Figure 5C was subject to bisulfite sequencing of the off-target binding sites at *Vac14* and *Tenm4* loci. Shown is the mean percentage ± SD of two biological replicates.

(G) Genomic DNA from cells used in Figure 1D and Figure 2C was subject to bisulfite sequencing of the off-target binding sites at *Vrk1* and *Gm42619* loci. Shown is the mean percentage ± SD of two biological replicates.

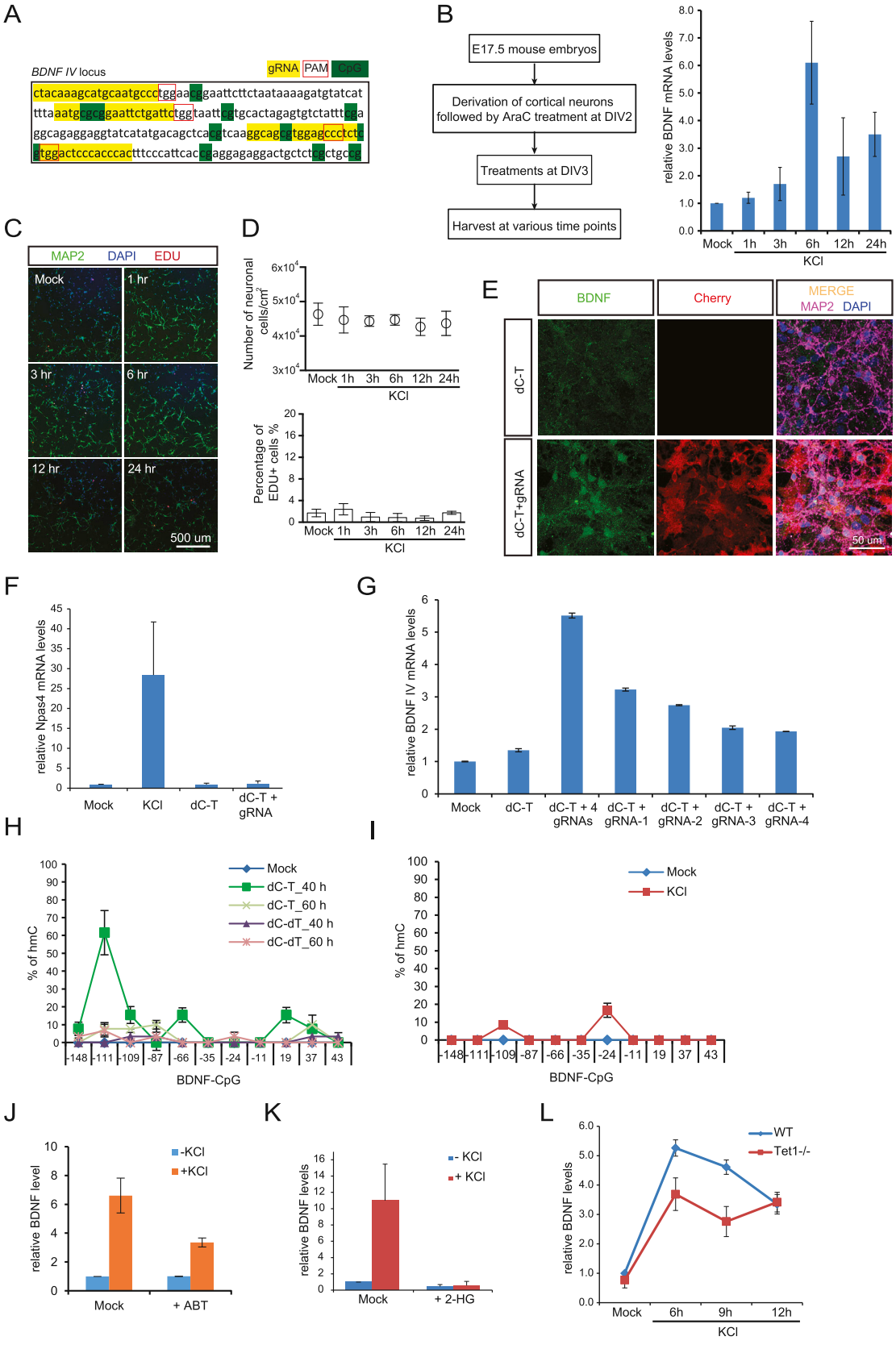


(legend on next page)

**Figure S4. Targeted Demethylation of *BDNF* Promoter IV by dCas9-Tet1 in Neurons, Related to Figure 3**

(A) Genomic sequence of the *BDNF* promoter IV region with gRNA sequences labeled in yellow and CpGs in green. PAM for each gRNA is highlighted by a red box.

(B) Left panel, schematic diagram depicting the KCl treatment and lentiviral delivery experiment on E17.5 mouse primary cortical neurons to investigate BDNF expression. Note that cultured neurons were treated with AraC on DIV2 to halt cell division in glial cells and neural progenitors. Right panel: DIV3 mouse cortical neurons were treated with 50 mM of KCl, and harvested at different time points for *BDNF* expression analysis by RT-qPCR.

(C) EDU labeling analysis for the mouse primary neurons over the course of KCl treatment for 24 hr. Note that extremely few EDU positive cells were observed. Stained in red for EDU, green for MAP2 and DAPI for nuclei. Scale bar: 500 um.

(D) Upper panel, quantification of neuronal density over the course of KCl treatment. The post-mitotic neuron density remains steadily around $4.5 \times 10^4/cm^2$ over time. Bars represent mean ± SD of three experimental replicates. Lower panel, quantification of the EDU positive cells over the course of KCl treatment. Less than 2% of the cells are EDU-pistive over 24 hr. Bars represent mean ± SD of three experimental replicates.

(E) Confocal micrographs of BDNF induction by ectopic expression of dCas9-Tet1 and a set of 4 gRNAs targeting *BDNF* promoter IV. Stained in green for BDNF, magenta for MAP2, red for Cherry and blue for DAPI. Note that the lentiviral infection efficiency is close to 100% in these neurons. Scale bar: 50 um.

(F) Neurons harvested from B and E were subjected to RT-qPCR analysis for Npas4 expression. Bars represent mean ± SD of three experimental replicates.

(G) DIV3 mouse cortical neurons were infected with dC-T alone or together with 4 gRNAs targeting *BDNF* promoter IV or individual *BDNF* gRNA, and then subject to qPCR analysis for BDNF expression.

(H-I) Tet Assisted Bisulfite sequencing (TAB-Seq) analysis of neurons infected with lentiviruses expressing dC-T or dC-dT with 4 BDNF gRNAs for 40 and 60 hr in H, or neurons after KCl treatment for 6 hr in I.

(J) DIV3 mouse cortical neurons were treated with ABT (50 uM) for 6 hr and then treated with KCl (50 mM) for 6 hr before harvest for RT-qPCR analysis. Bars represent mean ± SD of three experimental replicates.

(K) DIV3 mouse cortical neurons were treated with 2-Hydroxyglutarate (10 mM) for 2 hr and then treated with KCl (50 mM) for 6 hr before harvest for RT-qPCR analysis. Bars represent mean ± SD of three experimental replicates.

(L) DIV3 mouse cortical neurons derived from wild-type or Tet1 knockout E17.5 embryos were subject to time course KCl treatment experiments (6, 9 and 12 h). Bars represent mean ± SD of three experimental replicates.

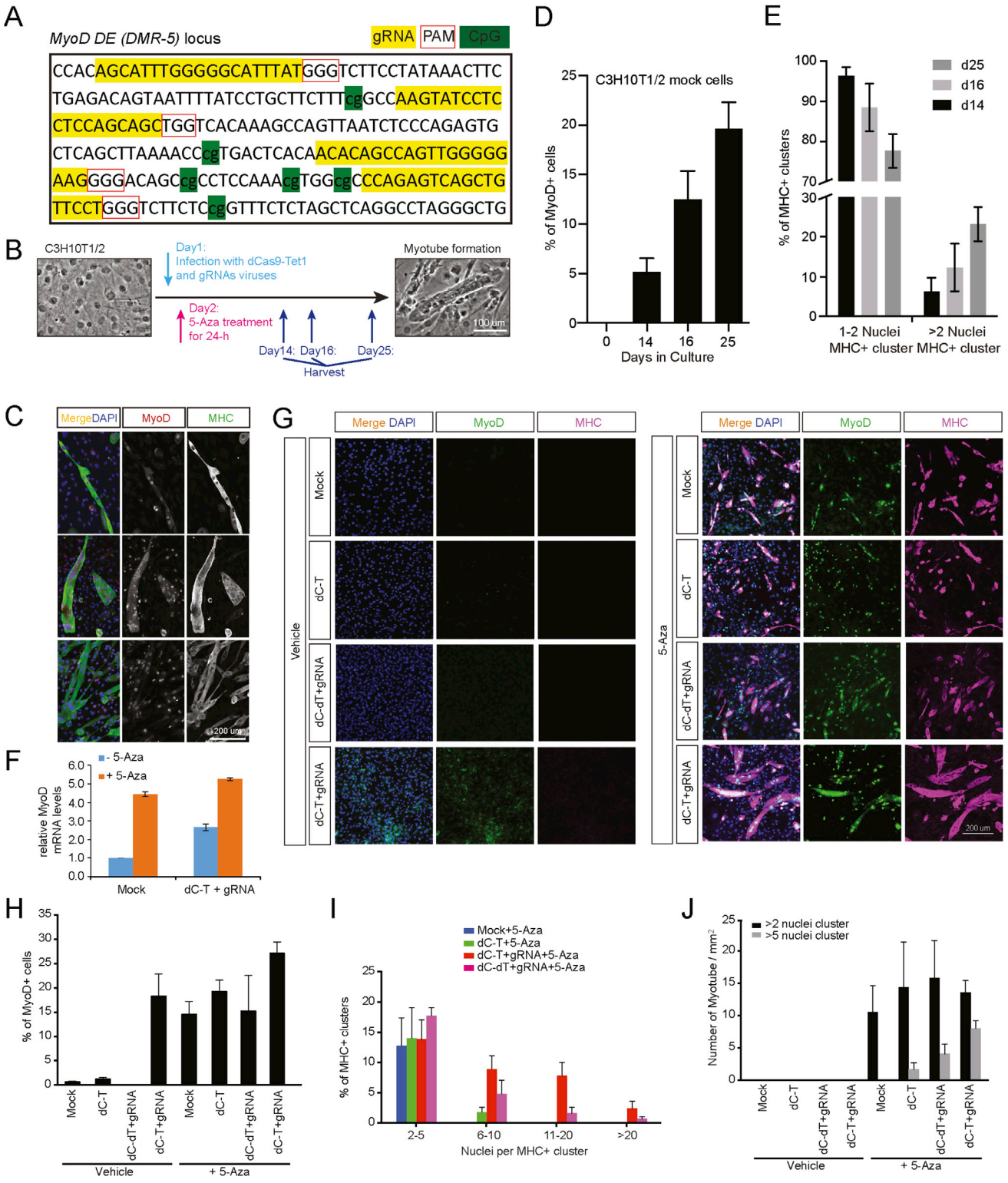


**Figure S5. Targeted Demethylation of the *MyoD* DMR-5 by dCas9-Tet1 and Conversion of Fibroblasts to Myoblasts, Related to Figure 4**

(A) Genomic sequence of the *MyoD* distal enhancer region with gRNA sequences labeled in yellow and CpGs in green. PAM for each sgRNA is highlighted by a red box.

(B) Experimental scheme of the fibroblast-to-myoblast conversion assay. Briefly, C3H10T1/2 mouse embryonic fibroblast cells were plated as $1 \times 10^4$ cells per well in 6-well plate, and then infected with lentiviruses expressing dCas9-Tet1 and target gRNAs. 24 hr post infection, cells were optionally treated with 5-Aza

*(legend continued on next page)*

(1 uM) for 24 hr (labeled in red), and harvested for immunofluorescence staining at different time points (day-14, −16 and −25, labeled in dark blue) with medium change every other day. Scale bar: 100 um.

(C) Representative confocal micrographs of myotube formation for C3H10T1/2 fibroblast cells after 5-Aza treatment. Upper panel: a clonal field contains sparsely distributed small and mid size myotubes. Middle panel: a clonal field contains sparsely distributed large size myotubes. Bottom panel: a clonal field contains high density of myotubes with heterogeneous size. Stained in green for MHC, red for MyoD and blue for DAPI. Scale bar: 200 um.

(D) Fraction of mock C3H10T1/2 cells expressing MyoD at different times after 5-Aza treatment. The fraction of cells expressing MyoD increases from around 6% at day 14 to around 13% at day 16 and reached around 20% at day 25. Bars represent mean ± SD.

(E) Number of nuclei in MHC+ cell clusters (grouped as 1-2 and > 2 nuclei per MHC+ cluster). Formation of larger myotubes was observed at later time points after 5-Aza treatment. Bars represent mean ± SD. Data was quantified from 3-5 representative images for each group in D and E.

(F) C3H10T1/2 cells were infected with lentiviruses expressing dC-T with *MyoD* gRNAs for 24 hr, and treated with or without 5-Aza for 48 hr before harvested for qPCR analysis. Bars represent mean ± SD of three experimental replicates.

(G) Representative images for C3H10T1/2 cells 16 days after infection with lentiviruses expressing dC-T and gRNAs targeting DMR-5 (*MyoD* distal enhancer) in a fibroblast-to-myoblast conversion assay as described in B. Note that a modest level of MyoD activation (compared to the cells treated by 5-Aza) was observed in cells with dC-T and target gRNA, but not myosin heavy chain (MHC) expression or myotube formation. Stained in magenta for MHC, green for MyoD and blue for DAPI. Scale bar: 200 um.

(H) Fraction of MyoD positive cells 16 days after infection with lentiviruses expressing dC-T alone or with gRNAs targeting DMR-5.

(I) Number of nuclei in MHC+ cell clusters (grouped as 2-5, 6-10, 11-20 and > 20 nuclei per MHC+ cluster) 16 days after infection. When treated with 5-Aza, co-expression of gRNAs and dC-T significantly facilitated formation of larger and more maturated MHC+ clusters compared to mock control or dC-T alone.

(J) Myotube density of MHC positive clusters with more than 2 or 5 nuclei 16 days after infection. Addition of 5-Aza induces MHC+ myotube formation. Co-expression of dC-T and gRNAs significantly induced more and larger myotubes (> 5 nuclei MHC+ clusters). Data are quantified from 3-5 representative images for H-J. Bars represent mean ± SD.

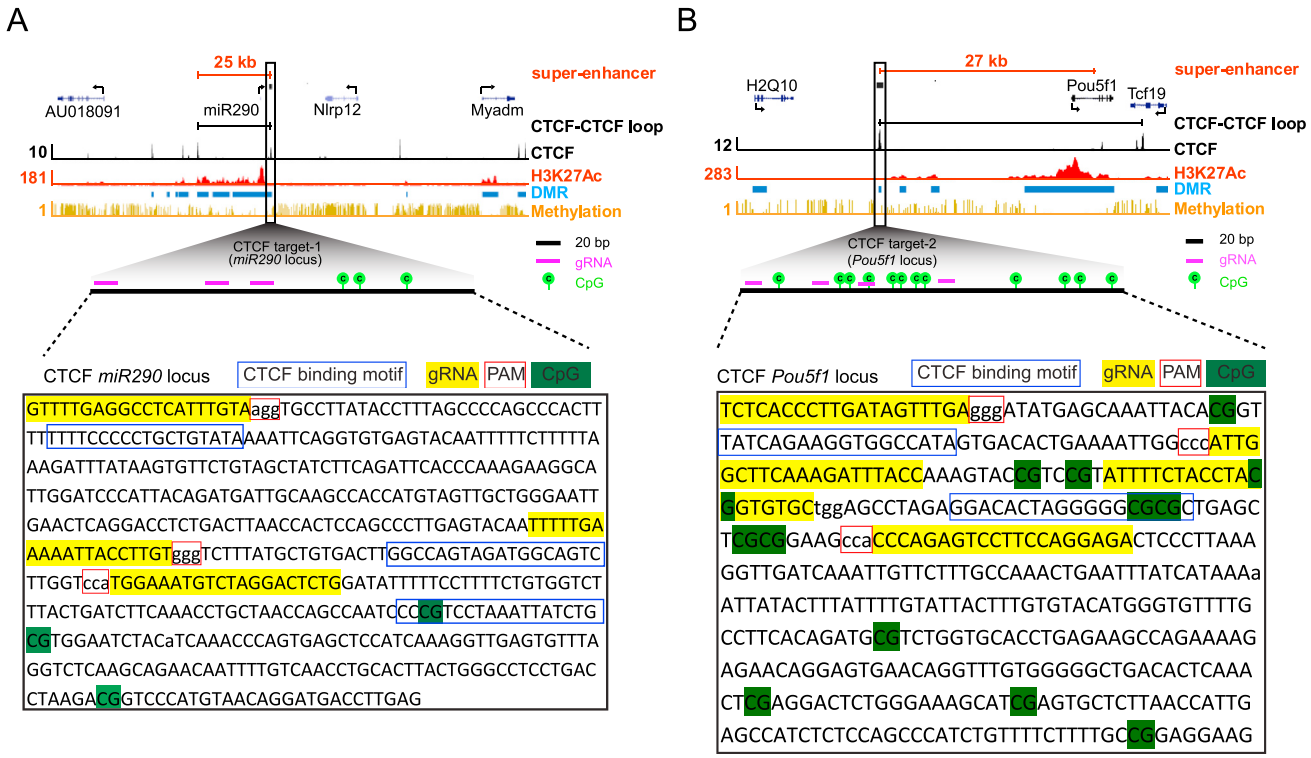


**Figure S6. gRNA Design for Targeted Methylation of CTCF Binding Sites for *miR290* and *Pou5f1* Loci, Related to Figure 5**

(A) Genomic sequence of the CTCF target 1 region (*miR290* locus) with gRNA sequences labeled in yellow and CpGs in green. PAM for each sgRNA is highlighted by a red box, predicted CTCF binding motif is highlighted in a blue box.

(B) Genomic sequence of the CTCF target 2 region (*H2Q10-Pou5f1* locus) with gRNA sequences labeled in yellow and CpGs in green. PAM for each sgRNA is highlighted by a red box, predicted CTCF binding motif is highlighted in blue boxes.

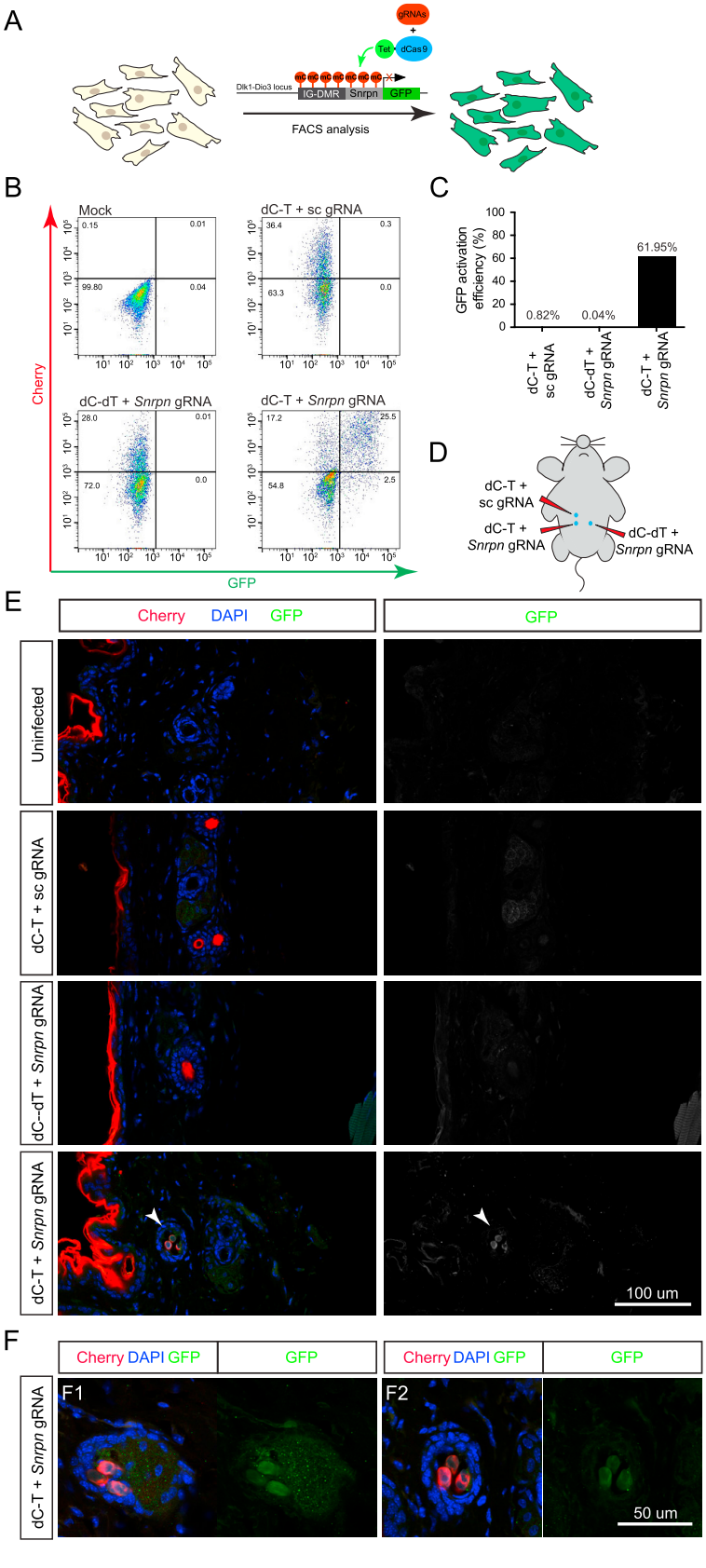


(legend on next page)

**Figure S7. Activation of IG-DMR$^{GFP/Pat}$ Reporter in Mouse Skin Cells by dCas9-Tet1-Mediated Demethylation, Related to Figure 6**

(A) Schematic diagram illustrating the experimental procedure for ex vivo activation of the silenced GFP reporter in IG-DMR$^{GFP/Pat}$ mouse fibroblasts. The cultured fibroblasts were infected with lentiviral vectors expressing dCas9-Tet1 and gRNAs to demethylate the *Snrpn* promoter and activate the GFP reporter.

(B) FACS analysis of the infected IG-DMR$^{GFP/Pat}$ mouse fibroblasts.

(C) Quantification of the percent of GFP+ cells in Cherry positive cell population in B.

(D) Schematic diagram illustrating the lentiviral delivery approach for each site on the ventral side of the IG-DMR$^{GFP/Pat}$ mouse.

(E) Representative confocal micrographs for the IG-DMR$^{GFP/Pat}$ mouse skin infected with dCas9-Tet1 and sc gRNA, an inactive form of Tet1 (dC-dT) and the *Snrpn* gRNAs, and dCas9-Tet1 with *Snrpn* gRNAs. Arrowheads indicate that only dC-T with *Snrpn* gRNAs activated the GFP expression. Note red auto-fluorescence on the left edges of the epidermis.

(F) Representative confocal micrographs of 2 hair follicles with lentiviral delivery for dC-T and *Snrpn* gRNAs to activate the GFP expression.